

AC  
.H3  
no.K76

Magnetic variations (2-30 cpd) on Hawaii  
AC .H3 no.K76 15384



Klein, Douglas Pyner  
SOEST Library

THESIS

070  
Kle  
Mag  
Ph.D.

MAGNETIC VARIATIONS (2-30 cpd)  
ON HAWAII ISLAND  
AND MANTLE ELECTRICAL CONDUCTIVITY

Douglas P. Klein

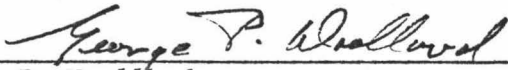
June 1976

Prepared for the National Science Foundation under  
Grant DES 75-05759 and submitted to the Graduate  
Division, University of Hawaii in partial fulfillment  
of the requirements for the degree of Doctor of  
Philosophy.

Approved by:

George H. Sutton, Principal Investigator

James C. Larsen, Co-Principal Investigator

  
George P. Woollard

Director, Hawaii Institute of Geophysics

MAGNETIC VARIATIONS (2-30 cpd)  
ON HAWAII ISLAND  
AND MANTLE ELECTRICAL CONDUCTIVITY

A DISSERTATION SUBMITTED TO THE GRADUATE DIVISION OF THE  
UNIVERSITY OF HAWAII IN PARTIAL FULFILLMENT  
OF THE REQUIREMENTS FOR THE DEGREE OF

DOCTOR OF PHILOSOPHY  
IN GEOLOGY AND GEOPHYSICS

AUGUST 1976

By

Douglas Pyner Klein

Dissertation Committee:

George P. Woollard, Chairman  
Augustine S. Furumoto  
James C. Larsen  
Gaylord Miller  
George H. Sutton

## ABSTRACT

Naturally occurring magnetic variations (2-30 cpd) observed by an array of magnetometers on the island of Hawaii are used to compute estimates of the complex and frequency dependent  $Z$  over  $H$  response functions. These data contain information about the electrical conductivity structure at depth in the mantle but are also strongly affected by the conducting ocean. The lateral contrast in electrical conductivity between the island-mass and sea-water produces large amplitude spatial gradients in the observed  $Z$  variations. These spatial distortions are related to a local horizontal deflection pattern in electrical current which is induced over a large region in the conducting ocean and which is coupled to the deep conductivity by mutual induction. This mutual induction is accounted for in the analysis of the  $Z$  over  $H$  response to estimate the deep conductivity structure. The spatial distortions are studied by comparing the response estimates between different observation sites. For each site the response function defines a direction for  $H$  where the  $Z:H$  coherence is maximized. This axis of principle induction is found to be generally perpendicular to the coast at each station. When rotated into their local direction of principle induction the response functions for frequencies less than 30 cpd at each site are found to relate to a reference site by a real and frequency independent transfer parameter. This result is interpreted to indicate that the ocean caused field distortions are essentially static for the lower

frequencies. Except for a constant multiplier at the reference site the spatial distortions are thus defined by the set of transfer parameters for the different stations. The unknown reference site parameter is determined simultaneously with the modeling of the observed response to the deep conductivity structure. General consistency is found between the estimated response and the theoretical response of the conductivity distribution determined by J. C. Larsen (1975) for Oahu.

## ACKNOWLEDGMENTS

This investigation began in 1968 under a United States-Japan Scientific Cooperation Program sponsored under the National Science Foundation (NSF) grants GA-1653 and GF-297. The program continued under NSF grants GF-402, GZ-48 and DES 75-05759.

The progress of the study, leading at this stage to the present dissertation, is due in large part to the guidance and unselfish contributions of many besides the author. The committee people, listed on the title page are foremost among these. I single out with gratitude Dr. George P. Woollard as the key person who encouraged the development of this program. Dr. Jim C. Larsen also receives special acknowledgment for generously sharing his ideas on the problems of oceanic electromagnetic induction. Others who contributed to various stages in this investigation include Dr. John C. Belshé who suggested the experiment, and Dr. Alexander Malahoff.

Dr. Tsuneji Rikitake and his associates, Dr. T. Yukutake, Dr. Y. Yamazaki, Dr. Y. Honkura, Mr. Y. Sasai and Mr. T. Yoshino, formed the collaborating group with whom the project began. They contributed the fluxgate magnetometers and assisted in the field work on the island of Hawaii. The hospitality and the creative scientific atmosphere they shared at the Earthquake Research Institute in Tokyo during the Japanese phase of the work are greatly appreciated. The theoretical modeling presented here is patterned after the numerical work of Mr. Sasai.

The Askania magnetometers were loaned to this project by the U. S. National Oceanographic and Atmospheric Administration (NOAA), and this organization also provided experimental testing facilities at Honolulu Observatory.

During the experiment on Hawaii Island, Dr. C. M. Fullerton opened the Cloud Physics Observatory in Hilo for one of our stations and, in addition, allowed the use of his laboratory for maintenance and calibration of our field equipment. The Honokaa Sugar Company, Honaunau Elementary School, the Hawaii State Agriculture Extension Service (Naalehu Office), the Hawaii Department of Land and Natural Resources (Pohakuloa State Park) and the 14th District U. S. Coast Guard Office all provided facilities for magnetometer stations.

Mr. Ralph Lavin and Mr. Dick Rhodes at the Hawaii Institute of Geophysics performed the painstaking drafting of illustrations for this report.

## TABLE OF CONTENTS

	Page
ABSTRACT . . . . .	iii
ACKNOWLEDGMENTS . . . . .	v
LIST OF ILLUSTRATIONS . . . . .	ix
LIST OF TABLES . . . . .	xi
1. INTRODUCTION . . . . .	1
2. THE NATURE OF MAGNETIC VARIATIONS ON ISLANDS . . . . .	6
3. THEORETICAL CONSIDERATIONS . . . . .	11
3.1 The Governing Equations . . . . .	11
3.2 A Generalized Working Model . . . . .	12
3.3 Some Relationships Describing Magnetic Variations on Mid-oceanic Islands . . . . .	14
4. THE METHOD OF ANALYSIS . . . . .	21
4.1 Some Preliminary Reductions . . . . .	21
4.2 The Principle Axis of Induction . . . . .	22
4.3 The Combined Response Spectrum . . . . .	26
5. MAGNETIC VARIATIONS ON HAWAII ISLAND . . . . .	28
5.1 Observational Data . . . . .	28
5.2 Sources of Error . . . . .	29
5.3 The Estimated Parameters of the Spatial Distortions . . . . .	30
5.4 The Estimated Response Spectrum . . . . .	35
5.5 Models of the Mantle Conductivity . . . . .	37
6. SUMMARY AND DISCUSSION . . . . .	47
7. CONCLUSIONS . . . . .	55
APPENDICES . . . . .	58

I	A MODEL OF ELECTRIC CURRENT AND MAGNETIC FIELD DISTORTIONS FOR HAWAII ISLAND . . . . .	58
	I.1 Theoretical Equations . . . . .	58
	I.2 Finite Difference Computations . . . . .	61
	I.3 Computation of the Vertical Magnetic Field . . . . .	64
	I.4 Modeling Results for Hawaii . . . . .	67
II	OBSERVED TIME SERIES AND RESPONSE SPECTRAL ESTIMATES . . . . .	73
	LITERATURE CITED . . . . .	80

## LIST OF ILLUSTRATIONS

		Page
Main Text		
Figure 1	A model of electric current and magnetic field distortions around Hawaii Island . . . . .	8
Figure 2	Magnetograms from the island of Hawaii . . . . .	10
Figure 3	The generalized conductivity model assumed in the present analysis . . . . .	13
Figure 4	Observed induction arrows on Hawaii Island . . . . .	34
Figure 5	The frequency response of the magnetic field fluctuations on Hawaii Island . . . . .	41
Figure 6	Conductivity models evaluated against the observational data . . . . .	43
Figure 7	"Best Fitting" conductivity-depth profiles . . . . .	44
Appendices		
Figure I.1	The grid convention for finite difference calculations . . . . .	58
Figure I.2	A flow chart of the finite difference procedure . . . . .	65
Figure I.3	A generalized conductance map of the Hawaiian Islands . . . . .	68
Figure I.4	A model of the regional electric current distortions near Hawaii . . . . .	70
Figure I.5	A model of the electric and magnetic field distortions for Hawaii Island . . . . .	71

Page

Figure II.1	The 24 hour time-series digitized at 4-minute intervals . . . . .	75
Figure II.2	The 52 hour time-series digitized over 10-minute means . . . . .	76
Figure II.3	The 12 day time-series digitized over hourly means . . . . .	77
Figure II.4	The transfer spectra estimates for each station . . . . .	78

## LIST OF TABLES

		Page
Main Text		
Table 1	Calculated and Theoretical Parameters of the Island Spatial Distortion . . . . .	31
Table 2	Combined Island Transfer Spectrum . . . . .	36
Table 3	Model I1 ( <u>Larsen</u> , 1975) . . . . .	40
Appendix 1		
Table II.1	Description of the Geomagnetic Observation Sites . . . . .	74

## 1. INTRODUCTION

An array of 3-component recording magnetometers was placed temporarily on the island of Hawaii to observe the time and spatial variations of natural magnetic fields. Here we report on the analysis of this data. The useful frequency range of this analysis is from about 2 to 30 cycles-per-day (cpd). The point of this investigation is to extract from the observed data the response function that can be used to interpret the pattern of electrical conductivity in the earth beneath Hawaii.

Time-varying magnetic fields originating from ionospheric current sources induce electric currents in the conducting regions of the earth and the oceans. Secondary magnetic fields resulting from these induced currents add to the primary fields. The induced currents themselves are internally affected by self-induction and coupled by mutual induction. The relationships among the components of the observed field reflect these electromagnetic interactions and would be predictable if the electrical properties of the earth were known. Conversely, a knowledge of the magnetic fields provides information about the electrical properties of the earth. The necessary physics is set up in Maxwell's equations and has been applied to geophysical studies for over 80 years (Schuster, 1889, Price, 1970).

Electromagnetic conductivity interpretations contribute to an understanding of the temperature sensitive structure of the earth, Tozer, 1959. The characteristically low conductivity of crystalline

materials which form the mantle at normal subcrustal temperatures increases dramatically at temperatures of about 1000°C and higher, Duba, Heard and Shock, 1974. Furthermore, a continuous fraction of highly conducting rock melt, even if present in amounts of only a few per cent, will alter the bulk electrical conductivity of a region upwards by more than an order of magnitude, Waff, 1974.

Such relationships suggest that the nature of the zone of decoupling between the earth's mobile lithosphere plates and the deeper mantle may be better understood by considering its electrical conductivity. A postulated mechanism for this decoupling is partial melting in the seismic low velocity zone of the mantle at about 100 km depth beneath the oceans, Anderson, Sammis and Jordan, 1972. If this is true a corresponding enhancement of electrical conductivity is expected. Another geophysical problem which can be better understood by integrating electrical conductivity interpretations with other data is the nature of the upper mantle beneath mid-oceanic islands. Mantle melting beneath volcanically active islands is not disputed as its result is observed at the surface volcanic vents, but the cause and extent of this melting is obscure.

The evidence and recent viewpoints regarding the origin of the Hawaiian Islands has been reviewed by Jackson, Silver and Dalrymple, 1972. A probable source depth for the basaltic magma is 60 to over 100 km. This conclusion is based on studies of the seismic activity associated with the recent eruptions, and also on studies of the volume and petrology of the island masses. The lateral diameter of

the magma source region is suggested to be about 300 km based on evidence of the surface distribution of volcanic vents. There is little geophysical evidence constraining the physical state of this source region; in particular, the volume and distribution of the ambient melt fraction and the temperature in this region is unknown. These parameters are required to develop an acceptable mechanism of melting, and any indications of abnormalities or otherwise from electrical conductivity interpretations would contribute to the problem.

Contrary to the fairly well studied electrical conductivity structure beneath large parts of the earth's continental regions, the body of direct knowledge available about the electrical properties beneath the ocean basins is largely limited to oceanic margins in a few areas, Schmucker, 1973. A recent remedial contribution in this regard is Larsen's (1975) electromagnetic investigation on Oahu Island, Hawaii. One notable result from this work is that the inferred electrical conductivity in the upper 300 km beneath the Oahu region generally resembles the normal continental results rather than the higher conductivity interpretations of the oceanic marginal areas (see Schmucker, 1973). This conclusion was also reached in a less exhaustive analysis of magnetic variation data from Oahu which indicated no unusually high subcrustal conductivities, Klein, 1972.

Equally important, in view of certain complicating relationships between electromagnetic field components on islands (see

below), Larsen, 1975, demonstrated how oceanic islands can be used as platforms for deep conductivity sounding. The present work supplements this result.

Oceanic-island magnetic fields are complicated by the fact that they strongly reflect the distribution of induced currents in the surrounding ocean. Seawater is one of the better electrically conducting material found naturally in large mass, while an island mass is essentially non-conducting. The island thus forms an obstacle to the flow of concentrated electrical currents induced in the seawater. The resulting distortion of the electric current pattern causes a corresponding disturbance of the magnetic fields.

Earlier investigations of island magnetic fields verified the existence of the disturbed magnetic field pattern and indicated its source, Mason (1963a, b; 1964), Elvers and Perkins (1964), Klein and Malahoff (1969). Other studies predicted the general pattern of disturbance using numerical models based on the conductivity distribution in the ocean as defined by bathymetric maps, Rogers (1966), Sasai (1968). Such models were used as a means to account for the disturbance fields and thus to estimate the magnetic effects of the deep mantle, Sasai (1968), Honkura (1971, 1973a, b), Klein (1971, 1972), Honkura et al. (1974).

In terms of interpreting the deep conductivity structure, these studies were not entirely satisfactory as the degree of coupling between the disturbance fields and the underlying mantle was not established by the models. The modeling assumption is that the

disturbance field can be treated as static and that it is essentially independent of mantle conductivity. Reasonable qualitative arguments can be made for this assumption under certain conditions, but an analytical basis for the assumption is not yet available. Until models are developed that include frequency dependent effects, or until there are firmer indications that such effects can be neglected the modeling approach must be used cautiously.

Larsen (1975) presented an alternative to the direct modeling of the disturbance fields as a means to account for the island disturbances. He used magnetotelluric data on Oahu to define all essential parameters of the disturbance field except one. This last unknown was included as a parameter to be determined in the final inversion of data which estimated the mantle conductivity by an iterative technique.

Larsen's basic approach is used here and is shown to be applicable to the analysis of island magnetic fields. The strength of this approach is that it derives from the data the principle information necessary to determine when and if the disturbance caused by the island can be reasonably separated from the mantle effect. It also indicates the frequency range for which the modeling approach might be valid and provides an empirical check on theoretical models of the disturbance field.

## 2. THE NATURE OF MAGNETIC VARIATIONS ON ISLANDS

It is convenient to consider magnetic variations on islands in 2 parts which are distinguished by their scale length: (1) the large scale magnetic response of the earth and ocean; and, (2) the perturbation of this large scale response by local inhomogeneities in the mantle and ocean. We refer to the second part as the locally disturbed fields associated with the island. These two parts are not generally independent because they can be coupled by mutual induction. The extent of coupling depends on the scale length of the local inhomogeneities and on the frequency of the fields. For example, a local conductivity inhomogeneity located in a surface layer is found to be negligibly coupled to deep conductors if its size is less than the depth to the highly conducting mantle material (Schmucker, 1971). In this case the local distortion pattern of the electromagnetic fields caused by the surface anomaly can be treated independently of the deep conductivity. The magnitude of the distorted fields, however, will be controlled in part by deep conductivity since it is related to the magnitude of the large scale and deeply coupled induction phenomena.

Numerical modeling of the perturbation for 2-dimensional surface structures like islands is usually based on the assumption of vanishingly small coupling effects between the mantle and the surface. Another common assumption is that the perturbation can be modeled as a static distortion of surface electric currents so that self-

induction is ignored. The qualitative justification for these simplifications is based on a dimensional analysis of the equation for electromagnetic induction in non-uniformly conducting thin sheets (eq. 10, Section 3.3; and see Appendix I). The parameter which describes the relative magnitude ratio of inductive effects to static galvanic effects involves a product of the scale length of the surface anomaly times the frequency of the electromagnetic fields, Price, 1949. For small inhomogeneities and/or low frequencies the assumption is taken to be valid. For Hawaii, it can be shown that this term indicates that the static approach would be considered valid for frequencies lower than about 10 cpd. Larsen (1975) finds from data obtained on Oahu Island that frequency dependent inductive effects become important for frequencies greater than about 6 cpd.

Figure 1 (left) shows a model of static electric currents as they would be disturbed by the island of Hawaii. This model is taken from the theoretical study described in Appendix I. The model assumes a uniform current pattern at the boundaries of the region of interest (located more than  $5^\circ$  from the edge of this figure). It is possible to visualize the general character of the disturbed vertical magnetic field by applying the right hand rule of thumb for electromagnetics. Observe that the direction of the disturbed vertical magnetic field will be opposed on opposite coasts of the island. The vertical field will vanish somewhere in the interior of the island producing a roughly antisymmetrical pattern as one crosses the island.

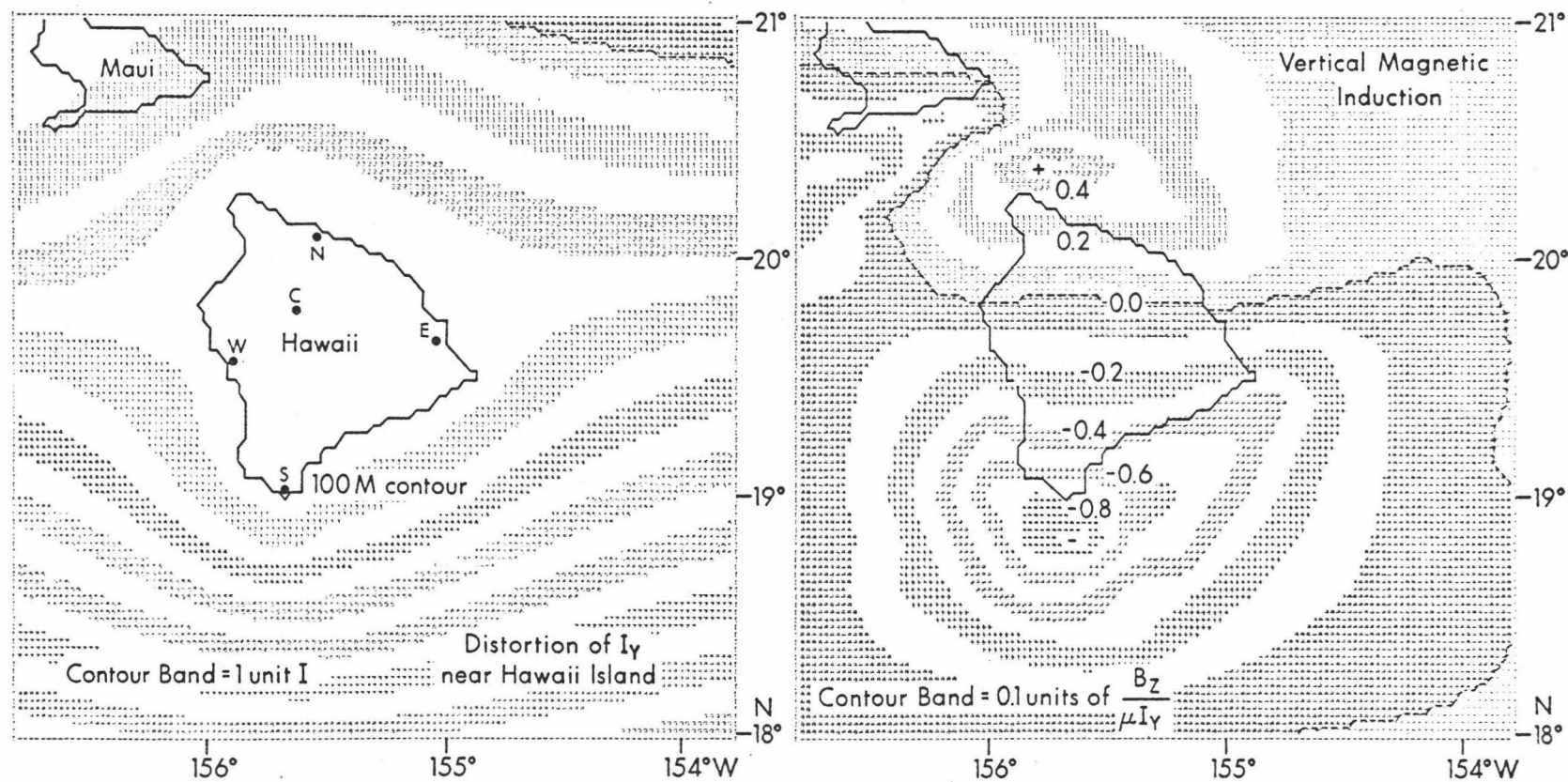


Figure 1. A model of electric current and magnetic field distortions around Hawaii Island. These represent the static perturbation of a uniform current sheet ( $I_y$ ) by the bathymetry around Hawaii Island. The contour bands of the electric stream function (left) can be interpreted as paths of equal current intensity. The units are arbitrary. The vertical magnetic field (right) is normalized as shown and is thus non-dimensional. The points indicated on the island are observational stations.

Figure 1 (right) shows a model of the vertical magnetic induction ( $Z = B_z$ ) as computed from the current distribution in Figure 1 (left). The magnetic field is normalized to the magnetic permeability times the magnitude of the uniform current intensity at the boundaries of the region.

Figure 2 show examples of magnetograms obtained on Hawaii Island at the stations marked on Figure 1. These illustrate the observed data and reveal the actual pattern of magnetic induction. It can be seen that the spatial disturbance predicted by the model agrees in general with the data. The horizontal components (D, H: magnetic east, north respectively) are reproduced from only one station because they are generally similar between sites (see the data in Appendix II for instance).

The induction pattern on Hawaii Island (Fig. 2) is typical of data published from previous island studies, Mason (1963a, b; 1964); Sasai, (1968); Honkura, (1973); namely, (1) the variations in the horizontal components are generally uniform across the island; (2) the magnitude of shorter period vertical variations is enhanced at near-coastal sites and decreases toward the interior; (3) the near-coastal vertical variations exhibit approximately  $180^\circ$  phase rotation on opposite sides of the island; and (4) the near-coastal variations in the vertical component are generally coherent with variations in that part of the horizontal component that is roughly normal to the nearest deep bathymetric contours.

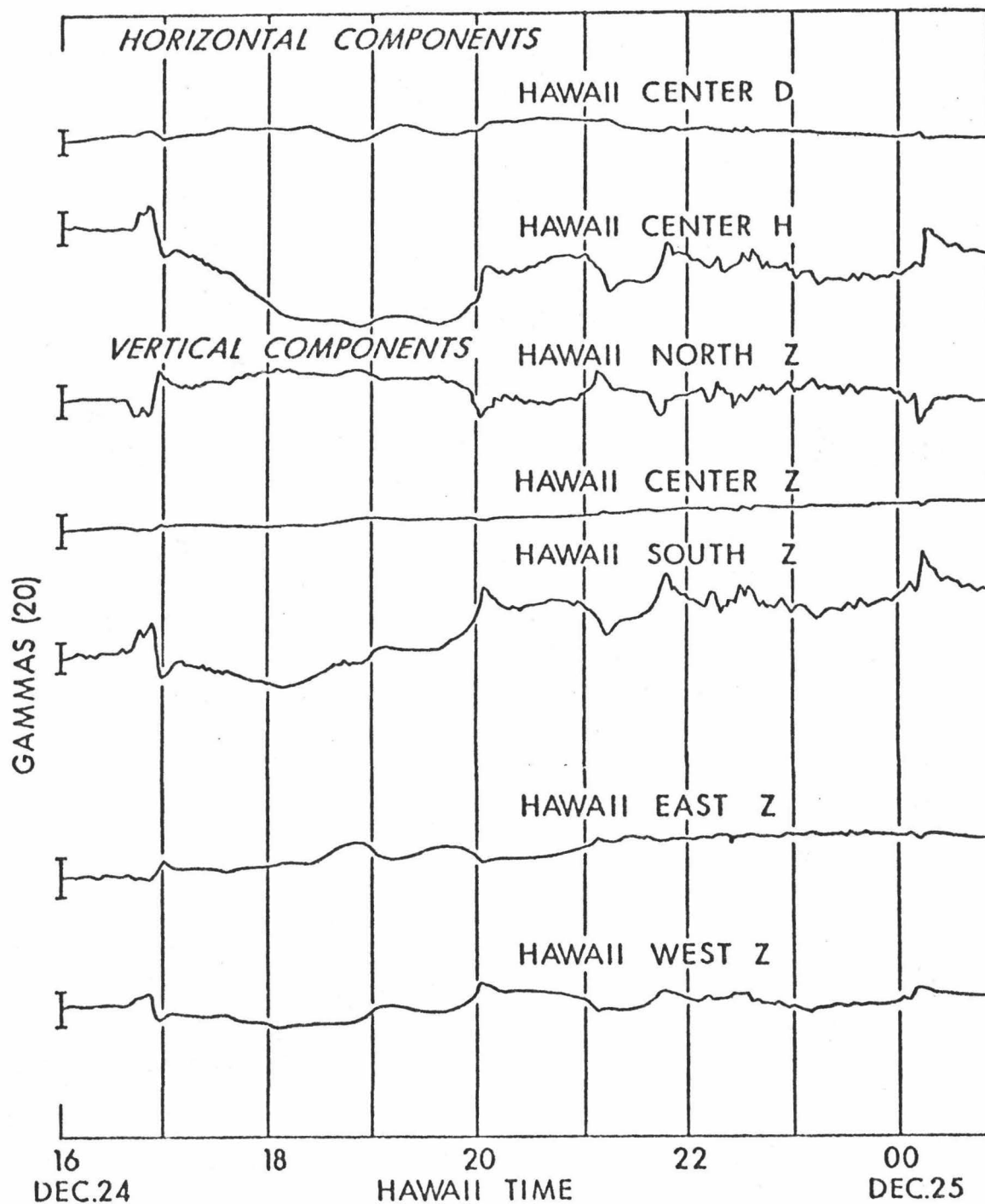


Figure 2. Magnetograms from the island of Hawaii. Note the generally anti-symmetric pattern of the vertical magnetic field (Z) on crossing the island. The stations designated by the data labeling are shown on Figure 1 (C, center; N, north; S, south; E, east; W, west). The horizontal magnetic variations are D, H (roughly magnetic east and north respectively).

### 3. THEORETICAL CONSIDERATIONS

#### 3.1 The Governing Equations

Electromagnetic equations will be expressed in rationalized mks units giving the fields as:  $\vec{E}$  (volts/m), electric field;  $\vec{B}$  (webers/m<sup>2</sup>), magnetic induction, which will be termed "magnetic field"; and  $\vec{J}$  (amperes/m<sup>2</sup>), current density. The observed  $\vec{B}$  fields will be expressed in the subsidiary units of gammas (1  $\gamma$  = 10<sup>-9</sup> webers/m<sup>2</sup>). The only material property of concern is the electrical conductivity ( $\sigma$ , mho/m) which is assumed to be isotropic. The magnetic permeability ( $\mu$ ) will be given its constant free space value ( $\mu_0 = 4\pi \times 10^{-7}$  Henry/m) which is appropriate for the bulk of earth materials, Tozer, 1959.

For slowly varying harmonic fields having an  $e^{i\omega t}$  time dependence ( $\omega = 2\pi f$ ,  $f$  is the frequency in Hertz), Maxwell's equations are written as:

$$\nabla \times \vec{B} = \mu \vec{J} \quad (1)$$

$$\nabla \times \vec{E} = -i\omega \vec{B} \quad (2)$$

These, in conjunction with Ohm's law,

$$\vec{J} = \sigma \vec{E} \quad (3)$$

and the conservation of current in source free regions,

$$\nabla \cdot \vec{J} = 0 \quad (4)$$

completely specify the electromagnetic fields in uniform regions. At the boundaries between differing regions the fields satisfy the conditions of continuity for the normal  $\vec{B}$  and  $\vec{J}$  fields and the tangential  $\vec{E}$  field.

### 3.2 A Generalized Working Model

Figure 3 shows a geophysical concept of the earth. The island is taken to be a non-conducting region in a thin layer which represents the ocean and its bottom sediments. This ocean layer is allowed to have variable conductance,  $\tau$ , near to the island, but is given a uniform conductance  $\tau_u$  at distant points. The conductance is defined as,

$$\tau = \int_0^d \sigma dz \quad (5)$$

where  $d$  is the ocean depth including the sediments. Following Larsen, 1975, the mean ocean depth far from the island  $d_u = 4.7$  km,  $\sigma$  of ocean water = 3.3 mho/m,  $\sigma$  of sediments = 1 mho/m. The thickness of the sediments is taken to be roughly 200 m. Thus  $\tau_u = 15,800$  mho.

The mantle is defined to include all space beneath the sediments. Its conductivity distribution is the primary unknown we seek. As a

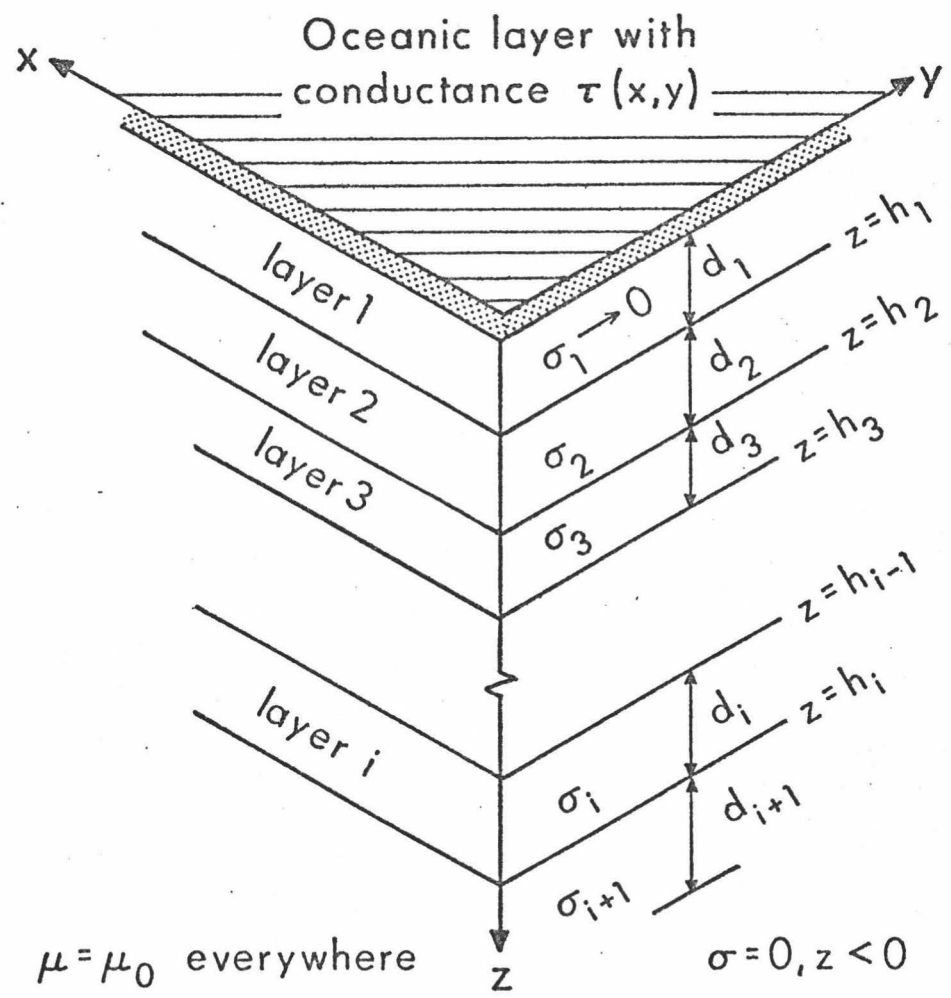


Figure 3. The generalized conductivity model assumed in the present analysis. The ocean is represented by a thin sheet of non-uniform conductance ( $\tau$ ) defined by the vertical integration of conductivity through the ocean. The "mantle" (shown as a layered medium) is assumed laterally uniform in conductivity ( $\sigma$ ) and non-conducting to a depth ( $d_1$ ) of a few tens of km below the ocean. The magnetic permeability is everywhere constant ( $\mu = \mu_0$ ).

preliminary constraint, the mantle conductivity will be allowed to vary only with depth, and the top few tens of km will be taken as essentially non-conducting.

### 3.3 Some Relationships Describing Magnetic Variations on Mid-oceanic Islands

The magnetic field components are expressed as

$$\vec{B} = \vec{H} + Z\vec{k}$$

where,

$$\vec{H} = X\vec{i} + Y\vec{j}$$

and  $\vec{i}$ ,  $\vec{j}$ ,  $\vec{k}$  are unit vectors in a right hand cartesian coordinate system with  $\vec{k}$  down.

The inducing fields are taken as uniform with respect to the scale of the island. Therefore island magnetic fields can be partitioned into the following two parts: (1) a uniform part,  $\vec{B}_u$ , which is associated with the external fields and their induction in the far ocean and mantle, and (2) an irregular part,  $\vec{B}_i$ , which is associated with the distortion of oceanic electric currents by the island.  $\vec{B}_i$  will vanish at points distant from the island.

The vertically integrated electric current density in the ocean will be described by the thin sheet counterpart of Ohm's law (eq. 3), Price (1949), as:

$$\vec{I} = \tau \vec{E} \quad (\text{amp/m}) \quad (6)$$

This is a valid approximation as long as the depth of the ocean is a small fraction of its skin depth  $(2/\omega\mu\sigma)^{1/2}$ , and also a small fraction of the radius of electromagnetic influence in the earth beneath the sea. A measure of this radius is the inductive scale length of the underlying mantle, real  $(E_x/i\omega B_y)$ , where  $\vec{B}$  and  $\vec{E}$  are measured at the sea floor, Schmucker, 1973. It should be noted that the ratio  $E_x/B_y$  (the "E over B response") at a given point is a complex and frequency dependent function of deep conductivity, Schmucker, 1973. For an isotropic, layered medium,  $E_x/B_y = -E_y/B_x$ , and when these ratios are divided by  $i\omega$  the resulting parameter (the "radius of induction") has the units of meters. For a uniform inducing field the real part of this parameter roughly indicates the depth of penetration as well as the horizontal distance of penetration of the electromagnetic fields observed at a specified point (Schmucker, 1973).

The sheet current density  $\vec{I}$  will also be partitioned into a uniform part  $\vec{I}_u$  and an irregular part  $\vec{I}_i$ , so that the  $\vec{B}$  and  $\vec{I}$  fields are given as:

$$\begin{aligned}\vec{B} &= \vec{B}_i + \vec{B}_u \\ \vec{I} &= \vec{I}_i + \vec{I}_u\end{aligned}\tag{7}$$

The thin sheet counterpart of eq. (1) is found by integrating vertically from  $z = 0$  to  $d$ , and applying the continuity conditions

across the sheet which represents the ocean. This gives for the horizontal fields,  $\vec{H}_i$  and  $\vec{I}_i = (I_{xi}, I_{yi})$  written as column vectors:

$$\vec{H}_i(0) - \vec{H}_i(d) = \mu \begin{pmatrix} 0 & -1 \\ 1 & 0 \end{pmatrix} \vec{I}_i \quad (8)$$

where  $\vec{H}_i(0)$  and  $\vec{H}_i(d)$  are the horizontal fields just above and just below the ocean layer respectively. If  $\vec{I}_i$  is the only electric current we expect that  $\vec{H}_i(0) \cong -\vec{H}_i(d_u)$  because of symmetry, thus the fields at the ocean surface are approximately given as:

$$\vec{H}_i = \frac{\mu}{2} \begin{pmatrix} 0 & -1 \\ 1 & 0 \end{pmatrix} \vec{I}_i \quad (9)$$

The thin sheet counterpart of eq. (2) is found by replacing  $\vec{E}$  by its expression from eq. (6) and applying the field separations, eq. (7), giving:

$$\nabla \times \frac{1}{\mathcal{T}} \vec{I}_i + i\omega \vec{B}_i = -i\omega \vec{B}_u - \nabla \times \frac{1}{\mathcal{T}} \vec{I}_u$$

By definition  $\vec{I}_u$  is constant and, far from the island,  $\mathcal{T} = \mathcal{T}_u$  where  $\mathcal{T}_u$  is constant. Thus, using the relation  $\nabla \times \frac{1}{\mathcal{T}_u} \vec{I}_u = -i\omega \vec{B}_u$  the above equation reduces to,

$$\nabla \times \frac{1}{\mathcal{T}} \vec{I}_i + i\omega \vec{B}_i = -\nabla \frac{1}{\mathcal{T}} \times \vec{I}_u \quad (10)$$

Since  $\vec{I}_i$  and  $\vec{B}_i$  are also related by an integral according to Biot-Savart's law (see Larsen, 1968), this equation (10) shows that either can be expressed in terms of  $\vec{I}_u$ . Thus,  $\vec{I}_u$  is considered as a driving term in eq. (10) which determines the magnitude of the current and magnetic field distortions. Eq. (10) can be used as a basis to numerically model the irregular part of the island fields, Price (1949); Rogers, 1966; Sasai, 1968; Bullard and Parker, 1970; Honkura, 1973, (and see Appendix I).

The vertical component of  $B_i$  can be expressed as:

$$Z_i = a\mu I_{yu} - b\mu I_{xu} \quad (11)$$

where  $a$  and  $b$  are position dependent parameters describing the parts of  $Z_i$  due to the distortion of the  $y, x$  components of  $\vec{I}_u$  respectively. The permeability,  $\mu$ , is kept separate so that  $a$  and  $b$  are nondimensional. These parameters are generally complex and frequency dependent, however, if the inductive term ( $i\omega \vec{B}_i$ ) in eq. (10) is of negligible magnitude these parameters will be real and constant.

As a first order approximation of  $\vec{I}_i$  a numerical solution of eq. (10) was found using the static ( $\omega = 0$ ) assumption. The spatial parameters ( $a, b$ ) were then found by numerically integrating Biot-Savart's law over the disturbing current distribution,  $\vec{I}_i$ . The resulting spatial parameters are listed in the following section. A description of the model is given in Appendix I.

Since  $\vec{I} = 0$  within the boundaries of a non-conducting island,  $\vec{I}_i = -\vec{I}_u$  according to eq. (7). Also, since  $Z_i$  is roughly anti-symmetrical across the island it is possible to choose a point at the "inductive center" where  $Z_i$  vanishes and where  $Z = Z_u$ . Letting  $Z_c$  and  $\vec{H}_c$  represent the vertical and horizontal magnetic fields respectively at the inductive center, we can replace  $\vec{I}_i$  in eq. (9) by  $-\vec{I}_u$  and combine the result with eq. (7) to give:

$$\vec{H}_c = \frac{\mu}{2} \begin{pmatrix} 0 & 1 \\ -1 & 0 \end{pmatrix} \vec{I}_u + \vec{H}_u \quad (12)$$

We now relate the observable fields,  $\vec{B}$  and  $\vec{B}_c$ , to the unknown uniform fields. The response parameter,  $Q$ , we use to form this relationship is a modification of the "E over B" response of the uniform fields defined by,

$$Q = -\mu \tau_u (E_{xu} / Y_u) = \mu \tau_u (E_{yu} / X_u) \quad (13)$$

By the definition of our deep conductivity model, which assumes horizontal uniformity and isotropy, we are justified in saying that  $(E_{xu}, X_u)$  are simple rotations of  $(E_{yu}, Y_u)$ . Then, since

$$\vec{I}_u = \tau_u \vec{E}_u, \text{ eq. (13) becomes}$$

$$\mu \vec{I}_u = Q \begin{pmatrix} 0 & -1 \\ 1 & 0 \end{pmatrix} \vec{H}_u \quad (14)$$

where  $\vec{I}_u$  and  $\vec{H}_u$  are considered as column vectors.  $Q$  is a nondimensionalized response of the earth at the ocean surface. This is the function

we seek which will allow us to interpret the deep mantle conductivity distribution. For a layered earth,  $Q$  has a known analytical expression, Wait, 1970; Schmucker, 1971, which will allow a straight forward modeling of the observed data.

Combining eqs. (14) and (11) gives:

$$Z_i = Q (a \chi_u + b \gamma_u) \quad (15)$$

Combining eqs. (14) and (12) gives:

$$\vec{H}_c = (1 + \frac{1}{2} Q) \vec{H}_u \quad (16)$$

and combining eqs. (15) and (16) results in the final expression:

$$Z - Z_c = q (a \chi_c + b \gamma_c) \quad (17)$$

where  $Z_i$  is written fully as  $Z - Z_c$  to point out the observables.

The function  $q$  is given by:

$$q = Q / (1 + \frac{1}{2} Q) \quad (18)$$

We thus have an expression, eq. (17), relating the observable island magnetic fields,  $Z$  and  $\vec{H}$ , the theoretical spatial parameters  $a$  and  $b$ , which must be determined, and the unknown mantle response  $Q$ . The latter is the primary function required to interpret the mantle conductivity structure. Observe that the function,  $q$ , could be defined as a modified mantle response without a loss of generality. However, since  $Q$  is widely used and easier to visualize (the normalized surface "E over B"), it shall generally be discussed as the primary unknown.

For an array of  $k$  stations, there will be  $2k + 1$  functions of frequency to be determined,  $(a,b)$  for each station, plus the unknown  $Q$ . This is assuming that for certain ranges of frequency,  $Q$  is a uniform function of frequency across the array. Initially, we shall not assume frequency independent  $(a,b)$ , but instead we will test the data to see if such an assumption is valid for any frequency interval. The next section will develop a method of analysis where first we can reduce the number of unknown spatial parameters to  $k + 1$  by a suitable rotation of data at each site of the array. Second, the data between stations will be related by a set of coefficients determinable from the data, which will effectively reduce the number of unknowns to two, one spatial parameter and  $Q$ . Then it will be possible to transfer all of the data to a single reference station and estimate a "combined" island response. If the array data are related by real and frequency independent coefficients (functions of  $a,b$ ) then we may separate the response  $Q$  from the spatial parameter at the reference site.

## 4. THE METHOD OF ANALYSIS

## 4.1 Some Preliminary Reductions

Let  $X_c$ ,  $Y_c$  and  $Z_{ik} = Z_k - Z_c$  be complex Fourier spectra.  $X_c$ ,  $Y_c$  and  $Z_c$  will be field components at the inductive center of the island. The subscript "k" will represent data from the kth perimeter station. This subscript will be deleted unless data combinations from different sites are indicated.

Equation (17) is rewritten as:

$$Z_i = T_x X_c + T_y Y_c + N \quad (19)$$

where, according to (17) and the model developed in the preceding section we have:

$$T_x = a q, \quad T_y = b q \quad (20)$$

$T_x$  and  $T_y$  are the initial island transfer spectra for each station k. N is the uncorrelated "noise" spectrum.

$T_x$  and  $T_y$  are estimated by minimizing the mean squared noise spectrum  $\langle NN^* \rangle$ , Schmucker, 1970. The brackets indicate the averaging operation over frequency and the asterisk designates the complex conjugate. The resulting equations, including the expression for the estimate of the squared residual  $E^2 = \langle NN^* \rangle / \langle Z_i Z_i^* \rangle$ , are:

$$\begin{aligned} T_x &= (S_{zx} S_{yy} - S_{zy} S_{xy}^*) / D \\ T_y &= (S_{zy} S_{xx} - S_{zx} S_{xy}) / D \\ E^2 &= 1 - (T_x S_{zx}^* + T_y S_{zy}^*) / S_{zz} \end{aligned} \quad (21)$$

where,

$$D = S_{xx} S_{yy} - |S_{xy}|^2$$

and the co-spectra terms, for instance  $S_{zx}$  which is the cross spectrum of  $Z_i$  with  $X_c$ , are given by,

$$S_{zx} = \langle Z_i X_c^* \rangle$$

If  $a$  and  $b$  were specified, for instance by a theoretical model study, the transfer spectra of eqs. (19) and (21) could be directly converted to the mantle response,  $Q$ , using eqs. (17, 18). This procedure would lead to estimates of  $Q$  for each perimeter site of the island. It is preferable however, to proceed further with the data analysis before calculating  $Q$ . The above approach implies  $2k$  degrees of freedom for possible model errors, resulting from the determination of  $(a, b)$  for each of the  $k$  sites. This leeway for possible misinterpretations of the effect of the surface layer can be improved by the following, which is similar to the approach taken by Larsen, 1975.

#### 4.2 The Principle Axis of Induction

From the initial transfer spectra, eqs. (19, 20), we find a horizontal rotation angle  $\theta$  which defines the azimuth of principle induction for each station. This rotation angle will define that component of the horizontal field variations which has maximum coherence with  $Z_i$ . For each site  $\theta$  is found by the maximizing  $\langle |T_u|^2 \rangle$  or the minimizing  $\langle |T_v|^2 \rangle$  where  $T_u$  and  $T_v$  are

defined by the rotation:

$$\begin{pmatrix} T_u \\ T_v \end{pmatrix} = \begin{pmatrix} \cos \theta & \sin \theta \\ -\sin \theta & \cos \theta \end{pmatrix} \begin{pmatrix} T_x \\ T_y \end{pmatrix} \quad (22)$$

$|T_u|^2$ , from eq. (22), can be written as:

$$\begin{aligned} 2|T_u|^2 &= |T_x|^2 + |T_y|^2 \\ &\quad - (|T_y|^2 - |T_x|^2) \cos 2\theta \\ &\quad + (T_x T_y^* + T_y T_x^*) \sin 2\theta \end{aligned} \quad (23)$$

By using the trigonometric identity:

$$D \cos 2\theta \pm S \sin 2\theta = (D^2 + S^2)^{1/2} \cos(2\theta \mp \varphi) \quad (24)$$

where,

$$\varphi = \tan^{-1}(S/D) \quad (25)$$

$|T_u|^2$  is found to have a maximum defined when  $\cos(2\theta + \varphi) = -1$ . Minimizing  $|T_v|^2$  in a similar manner generates the same analytical rotation angle,  $\theta$ . The desired result, estimated over frequency is:

$$\bar{\theta} = -\frac{1}{2} \tan^{-1} \left( \frac{\langle T_x T_y^* + T_y T_x^* \rangle}{\langle |T_y|^2 - |T_x|^2 \rangle} \right) + \frac{\pi}{2} \quad (26)$$

The overhead bar, in general, will indicate an estimated value of a parameter.

We point out that  $\bar{\theta}$  is ambiguous in the sense that  $\bar{\theta}$  or  $\bar{\theta} + 180^\circ$  are equivalent. This results from the fact that no account is taken of the direction of  $Z_1$  (up or down) in maximizing  $\langle |T_u|^2 \rangle$ , that is, the sign of  $T_u$  is ignored. For example, suppose that  $\bar{\varphi}$ , given by the inverse tangent in eq. (26), is equal to  $\pi$  (identical to  $-\pi$ ), then from (26):

$$\bar{\theta} = -\frac{1}{2} \bar{\varphi} + \frac{\pi}{2} = \begin{cases} 0, & \bar{\varphi} = \pi \\ \pi, & \bar{\varphi} = -\pi \end{cases}$$

The convention used here is to select that  $\bar{\theta}$  which rotates the horizontal field into a coordinate system where the component along  $\bar{\theta}$  is coherent with  $-Z_1$  (up). This puts the principle axis of induction into agreement with the sense of direction defined for the analogous "induction arrow", Everett and Hyndman, 1967.

A measure of the significance of  $\bar{\theta}$  is the ellipticity "angle",  $\epsilon$ , defined by:

$$\epsilon = \tan^{-1}(\bar{F} / 1 - \bar{F}) \quad (27)$$

where,

$$\bar{F} = \langle |T_v|_{min} \rangle / \langle |T_u|_{max} \rangle \quad (28)$$

and,

$$\begin{aligned}
 |T_v|_{\min}^2 &= \frac{1}{2}(T^2 - C^2) \\
 |T_u|_{\max}^2 &= \frac{1}{2}(T^2 + C^2) \\
 T^2 &= |T_x|^2 + |T_y|^2 \\
 C^4 &= |T_x|^4 + (T_x T_y^*)^2 \\
 &\quad + (T_y T_x^*)^2 + |T_y|^4
 \end{aligned}$$

If  $\epsilon$  is small then  $\bar{\theta}$  is well defined and it is justified to compute the principle axis transfer spectrum,  $T_u$ , which is defined by:

$$Z_i = T_u U_c + N \quad (29)$$

where,

$$U_c = X_c \cos \bar{\theta} + Y_c \sin \bar{\theta}$$

The  $T_u$  spectra are found by minimizing  $\langle NN^* \rangle$  to give:

$$T_u = S_{zu} / S_{uu} \quad (30)$$

and the squared residual:

$$E^2 = 1 - T_u S_{zu}^* / S_{zz}$$

The rotated spectra can be written in terms of the initial spectra by using the equations:

$$\begin{aligned}
 S_{zu} &= S_{zx} \cos \bar{\theta} + S_{zy} \sin \bar{\theta} \\
 S_{uu} &= S_{xx} \cos^2 \bar{\theta} + S_{yy} \sin^2 \bar{\theta} \\
 &\quad + (S_{xy} + S_{xy}^*) \sin \bar{\theta} \cos \bar{\theta}
 \end{aligned} \tag{31}$$

The spatial distortion of the magnetic field is now defined for each site by the rotation angle  $\bar{\theta}$  and a spatial parameter A, where:

$$T_u = Aq \tag{32}$$

When the axis of principle induction is well defined (small  $T_v$ ) we have the following relationships between (a, b) and (A,  $\bar{\theta}$ ):

$$\begin{aligned}
 A &= a \cos \bar{\theta} + b \sin \bar{\theta} \\
 \bar{\theta} &= \tan^{-1}(b/a)
 \end{aligned} \tag{33}$$

#### 4.3 The Combined Island Response Spectrum

Modified spatial parameters,  $R_k$ , which relate all data to a reference station, are defined by:

$$T_{uk} = R_k T_{ul} + N \tag{34}$$

where  $T_{ul}$  is the primary axis transfer spectrum at the reference site. Minimizing  $\langle NN^* \rangle$  over frequency leads to the estimate:

$$\bar{R}_k = \langle T_{uk} T_{ul}^* \rangle / \langle |T_{ul}|^2 \rangle \quad (35)$$

At this point, the spatial distortions of the magnetic field Z-component are completely specified by the observables,  $\bar{\phi}_k$  and  $\bar{R}_k$  for each perimeter station, and the theoretical parameter  $A_1$  at the reference station. Thus, using the  $\bar{R}_k$ , all data can be transferred to the reference site and combined to form an estimate of the island response spectrum  $T_{ul}$ . This new or combined  $T_{ul}$  is defined by:

$$Z_{ik} = R_k T_{ul} U_c + N \quad (36)$$

The combined estimate of  $T_{ul}$  is found by least squares as before giving:

$$T_{ul} = \frac{\langle \bar{R}_k^* S_{zu} \rangle}{\langle |\bar{R}_k|^2 \rangle S_{uu}} \quad (37)$$

with the squared residual,

$$E^2 = 1 - \bar{T}_{ul} \langle \bar{R}_k S_{zu}^* \rangle / \langle S_{zz} \rangle$$

In the above equations the co-spectra are associated with the components  $Z_{ik}$  and  $U_c$ . The summations are with respect to  $k$ . It finally remains to find the spatial parameter,  $A_1$ , which with  $T_{ul}$  will specify  $q$  by eq. (32) and the mantle response  $Q$  (eq. 18).  $Q$  is given by:

$$Q = T_{ul} / (A_1 - \frac{1}{2} T_{ul}) \quad (38)$$

## 5. MAGNETIC VARIATIONS ON HAWAII ISLAND

### 5.1 Observational Data

Simultaneous 3-component magnetic field recordings in geomagnetic coordinates were obtained at one centrally located and 4 perimeter stations on the Island of Hawaii (Fig. 1). The center station was an "Askania" variograph, the coastal stations were "Sokkisha" fluxgate magnetometers. The basic facts for each station are listed in Table 1 of Appendix II.

Two magnetically disturbed times (of 24 and 52 hour duration) and a 288 hour magnetically quiet time were selected for analysis. Data for the shorter events were available from all sites. These data were sampled at 4-minute intervals and by taking sequential 10-minute means for the 24 and 52 hour data sets respectively. The longer quiet time data, analyzed only for the central and southern stations, was sampled by taking sequential hourly means.

In the preliminary reduction, the time series were modified by eliminating the "drift" trends and rotating the components of each data set to geographic coordinates (x, north; y, east; z, down). For all time series except the x-component of the 288-hour data set, the drift correction was taken as linear and was based on the means of the first and last 10% of the series. The 288-hour x-component was modified by removing a 3rd degree polynomial curve fitted to the midnight values by the method of least squares. This non-linear trend was due to the recovery phase of a geomagnetic storm which occurred just prior to the sampling interval. The reduced time series are illustrated in Appendix II.

The time series were finally modified by a cosine fading function to minimize the errors in any remaining end truncations and were then transformed to the complex frequency domain by numerical Fourier series analysis.

## 5.2 Sources of Error

The Askania variograph at the center site had an internal Helmholtz coil system for periodic field calibrations and was used as the standard to define the variation amplitudes (in gammas,  $\gamma$ ). This instrument was calibrated against the standard magnetometers at Honolulu Observatory. The absolute amplitude error is estimated at roughly 3%.

Relative calibration factors between different instruments were obtained during a run of all instruments at the same site. From these tests the estimated error between instruments is about 3%. Digitizing errors are about  $\pm 0.2$  mm which results in additional scatter of about  $\pm 1 \gamma$  since the instrument sensitivities were 2 to 4  $\gamma$ /mm.

Further sources of discrepancy are drift in the instruments and temperature variations. These are difficult to estimate as long period instrument intercomparisons were not made. The former is probably linear and is believed adequately accounted for by the preliminary corrections to the time series. Temperature effects are negligible at the variograph station as the variograph was internally heated and temperature compensated. At the coastal sites these effects are expected to contribute to the uncorrelated residuals (in the range of 1 to 4 cpd) in the frequency domain analysis.

All of the above contribute to an estimated total error of about 10%. Timing errors are insignificant as field checks at 3-7 day intervals located discrepancies which were subsequently corrected prior to digitizing.

### 5.3 The Estimated Parameters of the Spatial Distortions

The inductive center of the island is taken as station C in Figure 1. This site was chosen on the basis of a pre-survey numerical model, Rikitake et al. (1969), which indicated that the static spatial parameters at this site were vanishingly small. Subsequent observations showed that oscillations in the vertical component of the magnetic field were conspicuously absent at this site for periods less than a few hours (see Fig. 2 and the data in Appendix II).

Cross-spectral estimates were made over frequency intervals of 1, 6, and 12 cycles/day (cpd) for the 188, 52 and 24 hour data sets respectively. Each estimate was independent with about 25 degrees of freedom. These cross spectra and the initial transfer spectra, eqs. (19-21), for the two shorter data sets were combined into a single set for each site. The long data set was considered separately as it was available only for one perimeter site.

The residuals ( $E$ ) of the initial transfer spectra, eq. (21), were taken as a measure of the significance of each harmonic estimate and used as weighting factors in the summations for the estimates of the principle axis of induction, eq. (26). The weighting factor for each

Table 1. Calculated and Theoretical Parameters of the Island Spatial Distortion

The theoretical parameters are predicted based on finite-difference modeling of static perturbations (see the text and Appendix I).

SITE	$\Delta f$ (cpd)	Calculated						Theoretical		
		$\bar{\theta} \pm \delta_1$	$\epsilon$	$\bar{r}$	real	$\bar{R}_k$ imag	$\delta_2$	$\theta$	$\hat{a}, \hat{b}$	$R_k$
S	1-30	$175^\circ \pm 11$	$9^\circ$	.14	1.0	0.0	--	$167^\circ$	- .63, .14	1.0
	36-60	$179^\circ \pm 7$	$7^\circ$	.11	1.0	0.0	--			
	66-156	$177^\circ \pm 9$	$10^\circ$	.15	1.0	0.0	--			
N	6-30	$-4^\circ \pm 7$	$7^\circ$	.10	.57	.008	.06	$27^\circ$	.22, .11	- .39
	36-60	$-9^\circ \pm 13$	$7^\circ$	.11	.54	-.04	.13			
	66-156	$8^\circ \pm 13$	$16^\circ$	.23	.52	-.03	.12			
E	6-30	$95^\circ \pm 2$	$5^\circ$	.08	.58	.02	.06	$98^\circ$	- .065, .47	.75
	36-60	$96^\circ \pm 8$	$4^\circ$	.06	.53	.13	.13			
	66-156	$96^\circ \pm 12$	$22^\circ$	.29	.47	.15	.21			
W	6-30	$234^\circ \pm 5$	$13^\circ$	.19	.51	.01	.05	$205^\circ$	- .29, - .135	- .50
	36-60	$237^\circ \pm 8$	$6^\circ$	.10	.54	.02	.10			
	66-156	$234^\circ \pm 13$	$11^\circ$	.16	.48	.12	.23			

Definition of the parameters. The equations refer to the main text.

$\Delta f$ : Frequency interval of the estimates.

$\bar{\theta}$ : Principle axis of induction relative to geographic north with rms error,  $\delta_1$ .

$\epsilon$ : "Ellipticity" associated with  $\bar{\theta}$ , eq. 27.

$\bar{r}$ : Ratio of transfer spectra along the minimum to the maximum axis' of induction, eq. 28.

$\bar{R}_k$ : Ratio of transfer spectra at site  $K = (N,E,W)$  to spectra at site  $K = S$  with the rms error,  $\delta_2$ , eq. 35, 42, 43.

$\hat{a}, \hat{b}$ : Theoretical spatial parameters, eq. 17, 20, 33.

harmonic  $j$  is specified as:

$$w_j = (1 - E_j)^2 \quad (39)$$

The principle axis of induction ( $\bar{\theta}$ ) at each site was estimated over the frequency bands 1-30, 36-60 and 66-156 cpd. These results with the respective rms errors,

$$\delta_j = \langle w_j (\theta_j - \bar{\theta})^2 \rangle^{1/2} \quad (40)$$

and estimated measures of ellipticity,  $\bar{\epsilon}$  and  $\bar{r}$  (eqs. 27, 28), are listed in Table 1. These azimuths are well defined (small  $\bar{\epsilon}$ ) and appear to be generally frequency independent over the frequency range of the data at each site.

The  $\bar{\theta}$  for the lowest frequency range at each site was used as the rotation angle in estimating the principle axis transfer spectra,  $T_{uk}$ , eq. (29). This selection was based on the consideration of possible frequency dependent characteristics (although not shown in  $\bar{\theta}$ ) and the larger estimated errors at higher frequencies.

The residuals associated with  $T_{uk}$  were used as weighting factors, as

$$w_j = (1 - E_j)(1 - E_1) \quad (41)$$

for the weighted least squares estimation of the modified spatial parameters, given as in eq. (34) by:

$$R_k = T_{uk} / T_{ul} \quad (42)$$

The south station data (S) was taken as a reference station for  $T_{ul}$ .

The resulting  $R_k$  with their weighted rms errors,

$$\delta_2 = \langle W_j | R_{kj} - \bar{R}_k |^2 \rangle^{1/2} \quad (43)$$

are given in Table 1.  $\bar{R}_k$  is seen to be generally real and constant with frequency. The variations in the real part of  $\bar{R}_k$ , and especially the increased imaginary part of  $\bar{R}_k$  with frequency are suspected to be indicative of the true behavior of the fields. However, these changes are not significant compared to the errors, and the primary conclusion from this data is that the spatial distortion on Hawaii island is predominantly phase and frequency independent up to 30 cpd.

The fundamental results are summarized on Figure 4. The arrow at each site indicates the principle axis of induction; its length is specified by the magnitude of  $\text{Re } \bar{R}_k$  ( $\text{Re} = \text{real part}$ ) for the 1-30 cpd data. The orthogonal axis at each site is proportional to  $\bar{r}(\text{Re } \bar{R}_k)$ , where, recalling eq. (28),

$$\bar{r} = \langle |T_v|_{\min} \rangle / \langle |T_u|_{\max} \rangle$$

and thus indicates the observed ellipticity of the fields. This representation is similar to the "induction arrow" of Parkinson, (1959) and Everett and Hyndman (1967), and the "vectored" principle axis points to the region containing the main concentration of source

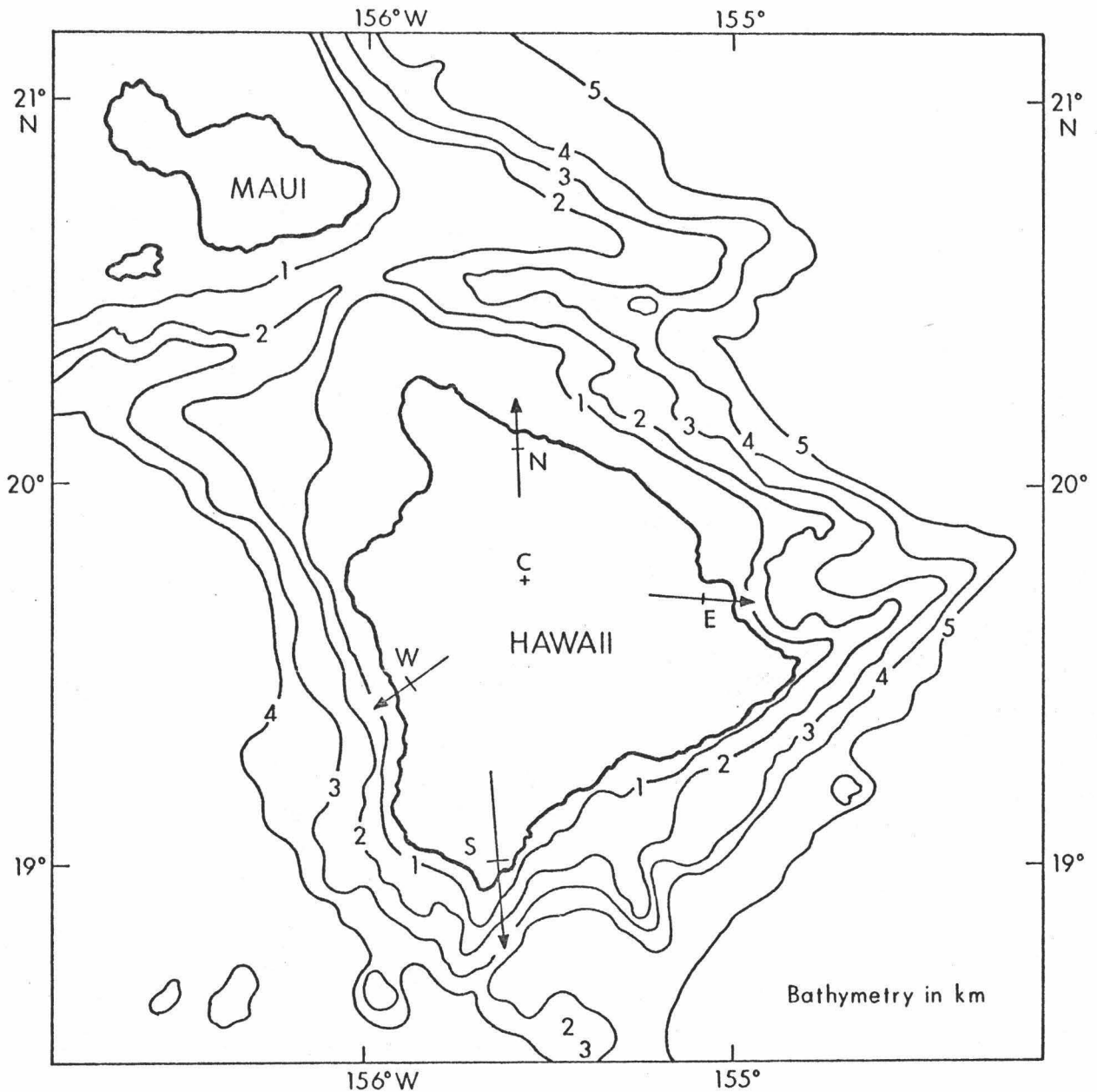


Figure 4. Observed induction arrows on Hawaii Island. These arrows represent the direction of maximum coherency between vertical (Z) and horizontal (H) magnetic fluctuations. The length of the arrows are proportional to the amplitude  $|Z/H|$ . The "ellipticity" of the fields (interpreted as the relative uncertainty in the direction) is indicated by the bars orthogonal to the arrows.

currents for  $Z_{ik}$ . It is evident that on Hawaii these regions are associated with the deep bathymetry surrounding the island.

Plots of the rotated spectral estimates  $T_u$  (eq. 29), are presented in Appendix II.

#### 5.4 The Estimated Response Spectrum

The real parts of  $\bar{R}_k$  were used to combine the data from all sites into a single set ( $\bar{T}_{u1}$ ) referenced to site S according to eq. (37). These island response estimates for the two combined shorter data sets are computed over independent 6 cpd intervals with about 100 degrees of freedom each. The long data set from site S provided 2 additional estimates centered on 2 and 5 cpd with about 75 degrees of freedom each. Because of the larger errors in the estimated  $\bar{R}_k$  for the higher frequency data (greater than 30 cpd) and the possibility that the assumption of real  $\bar{R}_k$  may not be valid at these higher frequencies only those estimates having frequencies less than or equal to 30 cpd are considered in the interpretative analysis.

The data ( $\bar{T}_{u1}$ ) with frequencies up to 54 cpd are listed in Table 2. A third degree polynomial was fitted to these data using  $\log f$  (cpd) as the independent variable. The rms error of the polynomial, assuming a circular error in the complex plane, was 0.11. This agrees with the mean of the estimated errors in Table 2 (0.14), and  $\pm 10\%$  to  $15\%$  is considered to be an overall estimate of the data consistency.

Table 2. Combined Island Transfer Spectrum

The mean root mean square (rms) discrepancy in the data (1-30 cpd) is .14. The rms error in the polynomial approximation is .11.

f (cpd)	Estimated Transfer Spectra			3rd Degree Polynomial Approximation	
	real	$\bar{T}_{u1}$ imag	$\delta$ rms error	real	imag
2.04	.207	- .326	.27	.218	- .326
5.04	.639	- .376	.18	.580	- .385
6.00	.625	- .378	.04	.640	- .376
12.25	.751	- .329	.14	.852	- .296
18.00	1.031	- .196	.07	.947	- .231
24.25	.901	- .219	.18	1.012	- .175
30.00	1.203	.002	.11	1.054	- .134
36.25	1.061	- .194	.22	1.089	- .0973
42.00	1.146	- .033	.28	1.114	- .0691
48.00	1.037	- .189	.26	1.136	- .0431
54.00	1.192	.084	.21	1.154	- .0228

### 5.5 Models of the Mantle Conductivity

The estimates of the island response spectra (2-30 cpd) referenced to station S (Table 2) are the basic data used for comparison to models of the mantle conductivity response. In the coordinate system (u,v) where u is along the axis of principle induction at site S, the island response T is related to an island distortion parameter A and the mantle response Q (defined in eqs. 13, 14) by the equations:

$$T = Aq \quad (32)$$

$$q = Q / (1 + \frac{1}{2} Q) \quad (18)$$

Neither A nor Q are known.

Here we estimate A simultaneously with the modeling of Q. Selected conductivity distributions for a horizontally layered mantle are used to compute a theoretical response  $Q_t$ . This is used in eqs. (18, 32) to estimate the best A (in the least-squared-residual sense) that fits  $q_t$  to T. When minimizing the weighted sum of squares,

$$\langle w | T - Aq_t^* |^2 \rangle \quad (44)$$

with respect to A the estimate is given by

$$\bar{A} = \langle w T q_t^* \rangle / \langle w | q_t^* |^2 \rangle \quad (45)$$

The summations are over the frequencies (1-30 cpd) listed in Table 2. The estimated errors in  $T$ ,  $\delta_j$ , also listed in Table 2, are used in weighting factors as

$$w_j = (1 - \delta_j)^2 \quad (46)$$

It was concluded in Section 5.3 that  $\bar{A}$  is real (phase independent) within the errors of the data. Thus we have defined the discrepancy between the model (including both  $\bar{A}$  and  $Q_t$ ) as:

$$D = \langle w | T - q_t \operatorname{Re} A |^2 \rangle^{1/2} \quad (47)$$

In all models we assume an isotropic mantle and an essentially uniform inducing field (spatial wave-number of  $10^{-6} \text{ m}^{-1}$ ) that has  $\vec{E}$  tangentially polarized with respect to the earth's surface (TE mode). Wait's (1970) algorithm (see also Schmucker, 1971) is used to compute  $Q_t^-$  at the sea floor. The observations are roughly in the plane of the sea surface so  $Q_t^-$  is continued upward to the sea surface to find  $Q_t$  by using the relationship (Larsen, 1975)

$$Q_t = -Q_t^- / (1 + Q_t^-) \quad (48)$$

The conductivity model L1 (Larsen, 1975), interpreted for the mantle beneath the island of Oahu (300 km northwest of the island of Hawaii) was logically the first conductivity distribution to be tested against the present data. Larsen derived this model by the

inversion of electromagnetic data in the frequency range of 0.1 to 6 cpd. The consistency of his data as indicated by extremely low error estimates is remarkable, and the model derived (listed in Table 3 of this paper) is unusual in that it has a well resolved anomalously high conductivity at about 300 km depth.

The  $\bar{A}$  (eq. 45) found using model L1 is (.831, .110) for the real and imaginary parts respectively. The model discrepancy, D (eq. 47) was .192. A second modeling was run using a "modified" L1 model where the conductivity anomaly (1.581 mho/m) was replaced by a conductivity of .27. Here  $\bar{A}$  and D were found to be only slightly modified, (.834, .111) and .194 respectively. A comparison of the responses  $Q_t$  between the L1 and L1 modified models demonstrated that no significant differences could be observed for frequencies above 10 cpd.

The theoretical island response  $T_t$  obtained using eq. (32) with  $Q_t$  (from model L1) and  $\bar{A} = .831$  is plotted along with the present data in Figure 5. The fit is reasonably good for frequencies below 10 cpd, but for the higher frequencies the imaginary part of response of the L1 model differs noticeably from the present data.

Observe also that the imaginary part of  $\bar{A}$  (approximately 0.1) is quite large and that the discrepancy D is larger than the mean estimated error in the data (.14, see section 5.4). The conclusion is that the present data may require a slightly different conductivity in the shallower layers than model L1.

Table 3. Model L1 (Larsen, 1975)

Layer	Layer thickness (km)	Conductivity mho/m
0	(thin-sheet)	( $\sigma_u d_u = 15,800$ mho)
1	65	.077
2	108	.093
3	154	.097
4	50	1.581
5	150	.270
6	121	.589
7	infinite	1.014

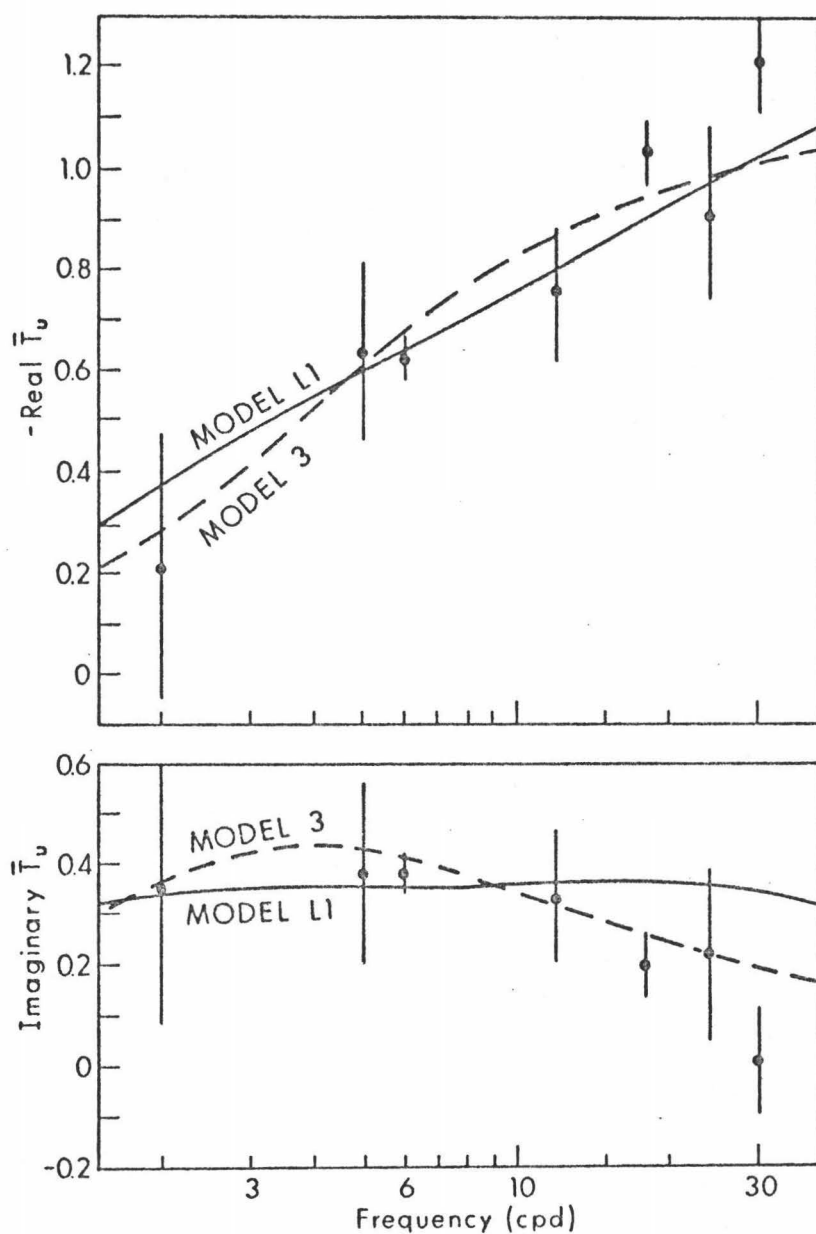


Figure 5. The frequency response of the magnetic field fluctuations on Hawaii Island. The estimated island response ( $\bar{T}_{u1} = Z/H$ ) referenced to the direction of principle induction at site S (see text) is indicated for the various frequencies with error-bars having twice the root-mean-square discrepancy computed for each estimate. The solid line is the theoretical response calculated on the basis of model L1 (Larsen, 1975, see Fig. 7 and Table 3). The dotted line is the theoretical response calculated on the basis of model 3 (Fig. 7).

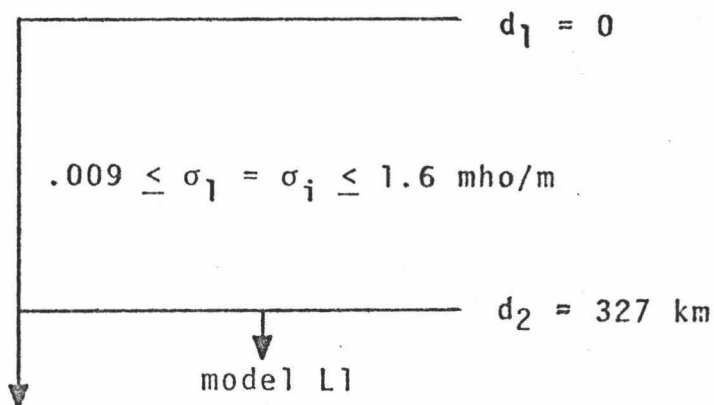
For further modeling, the response of a constrained set of models (Fig. 6) having 1 to 3 "overburden" layers above 327 km was compared to the data. Model L1 was retained as the conductivity distribution below 327 km. A total of 1360 model responses were generated and tested against the data.

The models having smaller errors of fit,  $D$ , showed generally lower conductivity at depths above about 300 km than model L1. Three illustrative models are shown in Figure 7. These examples are the best fitting homogeneous overburden (model 1), the best fitting 3-layer overburden (model 3), and the most conductive 2-layer overburden which has a modeling error,  $D \leq .140$  (model 2). A total of 21 different models within the set of Figure 6 showed an error,  $D \leq .140$ , which corresponds to the estimated mean error in the data (Table 2). The smallest  $D$  in this set was .137. In general, the magnitude of  $D$  decreased as the imaginary part of  $\bar{A}$  decreased. This result is expected since  $D$  was computed using the theoretical response,  $T_t$ , based on the real part of  $\bar{A}$  (eq. 47).

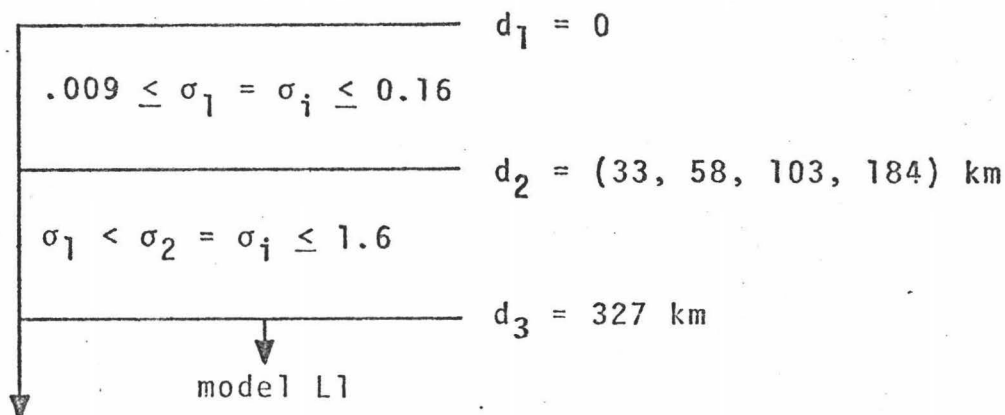
The estimated spatial parameters,  $\bar{A}$  (real, imaginary), are (.561, .012), (.620, .048) and (.590, .037) for the models 1, 2 and 3 respectively. These values are in good agreement with the predicted value of .64 (real), see Table 1 and eq. (33), for site S.

The theoretical response for the best 3-layer overburden model (3) is plotted in Figure 5 against the data and the response of model L1. The improved fit of model 3 compared to model L1 is apparent, especially in the higher frequency range of the spectrum.

## A. SINGLE LAYER OVERBURDEN



## B. TWO-LAYER OVERBURDEN



## C. THREE-LAYER OVERBURDEN

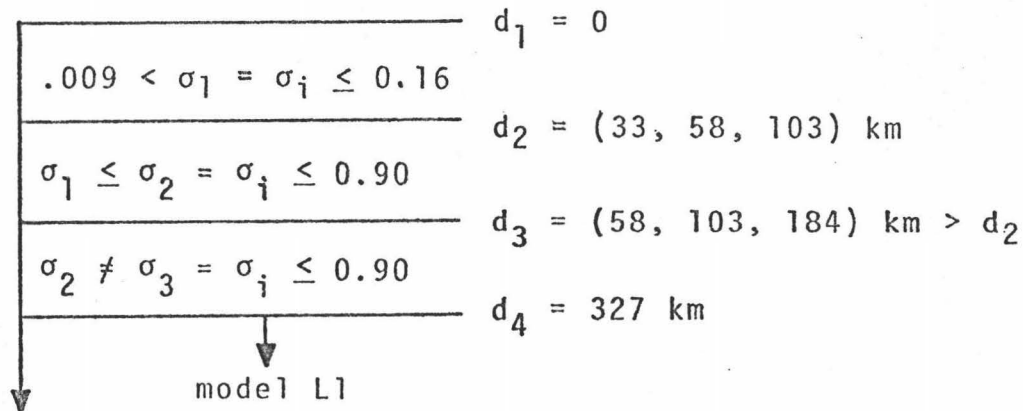


Figure 6. Conductivity models evaluated against the observational data. In all models tested the substrata below 327 km consisted of layers 4-7 of model L1 (Larsen, 1975, see Table 3). The overburden consisted of an "oceanic" sheet (conductance 15800 mho) underlain by 1 to 3 layers having interface depths and conductivities constrained as indicated here. The allowable conductivities,  $\sigma_i$ , were .009, .016, .028, .051, .090, .160, .280, .510, .900, 1.600 mho/m.

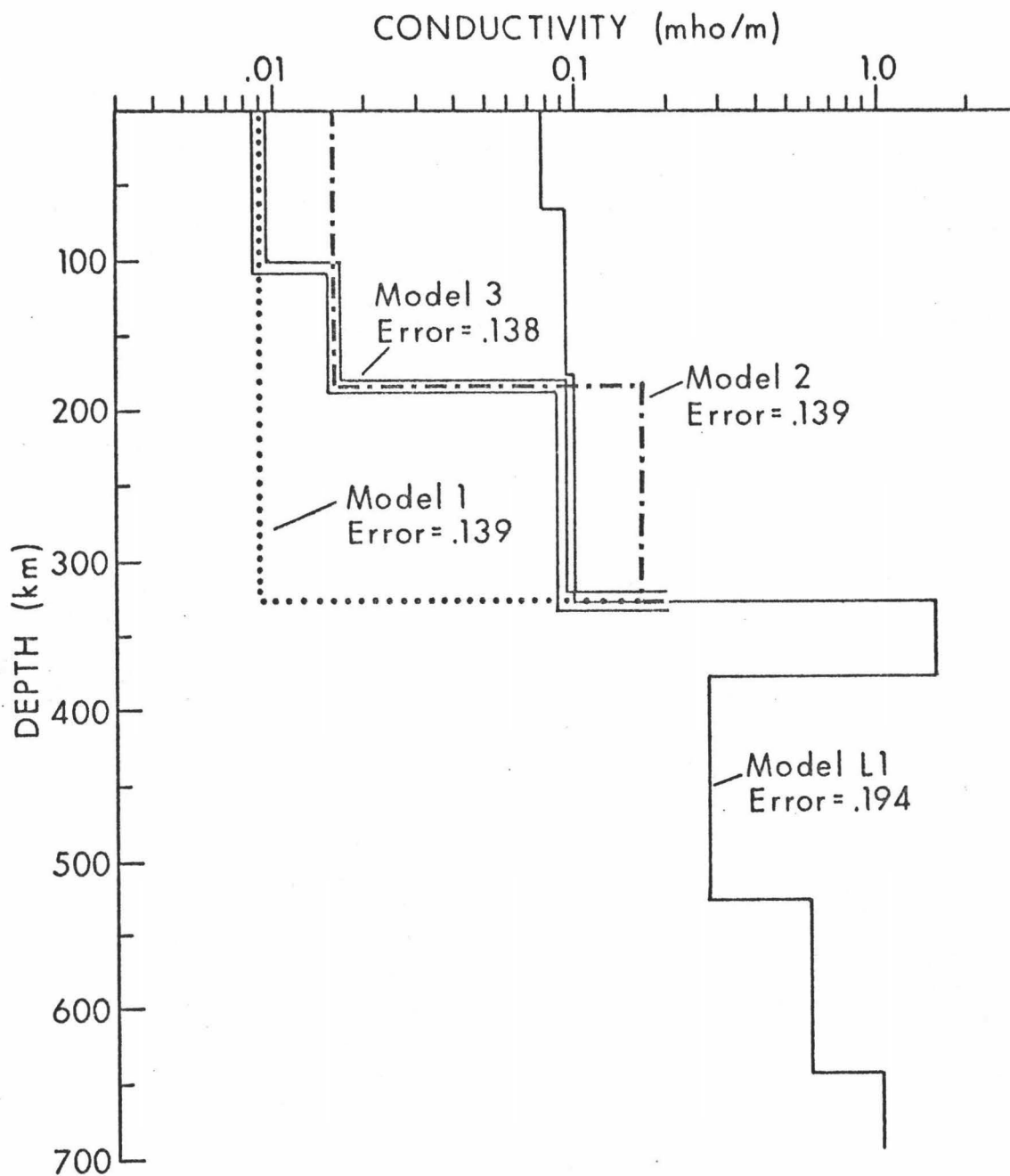


Figure 7. "Best Fitting" conductivity-depth profiles. The 3 models shown (exclusive of L1) are illustrative of those with relatively small errors of fit (see text). Model L1 (Larsen, 1975) is shown for comparison. The modeling is suggestive of a lower conductivity above about 180 km depth than model L1. Model 3 had the smallest error of fit of all models tested. Model 2 is the most conductive model having an error of fit less than 0.14 (typical of the data error, see text). Observe that there is virtually no definition of the minimum conductivity limit (e.g. model 1 is the least conductive model tested).

It is emphasized that model L1 was derived from data in the frequency spectrum of 0.1 to 6.0 cpd, thus the overlap between Larsen's (1975) data and the present data is only from 2 to 6 cpd. The agreement of the present data with the response of model L1 in this frequency range means that there is no evidence for a deep (greater than 300 km) conductivity inhomogeneity between Oahu Island and the island of Hawaii. The only evident difference between the present data and the L1 response is found in the frequency range of 10-30 cpd. These higher frequency data can define the shallower conductivity (100-200 km) better than Larsen's data, but they serve primarily as a means to supplement model L1 rather than indicating a difference in conductivity between Oahu and the island of Hawaii.

We interpret these modeling results to indicate an upper limit of about .02 mho/m in the mantle conductivity from 100-180 km depth beneath the region of Hawaii Island. From about 180 to 300 km the maximum conductive is indicated to be about 0.2 mho/m. The best fitting 3-layer model suggests a rise in conductivity at about 100 km, but considering the resolution of the data as indicated by the conductivity range between the equally well fitting models 1 and 2, this result is not given much credance.

The least conductive model in the set tested, model 1, fits the data as well as more conductive models up to the conductivity maximums discussed above. Thus we can not place a lower bound on the possible conductivity in the region above 300 km depth. Some supplementary models showed that the modeling error remains essentially

constant and low ( $< .14$ ) as the upper mantle is given vanishing small conductivity.

## 6. SUMMARY AND DISCUSSION

The analysis of island magnetic variations must account for a spatially non-uniform, ocean-induced signal as well as the mantle response. One means of accounting for the ocean-induced part is to predict it by numerical modeling. Larsen (1975) presented an alternative approach in which the ocean-induced field distortions are modeled as part of the overall response of the earth. Larsen used electric field data, but the method was adopted here for magnetic data. The theoretical basis of this approach which was developed in Sections 3 and 4 (eq. 32) is the equation:

$$Z_i / H = A q \quad (49)$$

where  $Z_i$  is the disturbed vertical magnetic field and  $H$  is the observed horizontal field oriented in the direction of the principle azimuth of induction (i.e. the direction of that component of the horizontal field having maximum coherence with  $Z_i$ ). The parameter  $A$  describes the amplitude of the ocean induced distortions of the fields, and  $q$  is essentially the electromagnetic response of the mantle. If  $A$ , which varies with location, is found to be real and frequency independent, and if  $q$ , which is complex and frequency dependent, can be supposed to be constant in the region of observations, then the two parameters can be separated. The data provide indications if the necessary conditions are met.

In applying eq. (49) it is necessary to estimate  $Z_i$ , the disturbed vertical magnetic field. The total observed vertical field is

$Z = Z_i + Z_u$  where  $Z_u$  is the undisturbed field. A first approximation would be to take  $Z_u$  as zero, since the amplitude of  $Z_u$  is proportional to the spatial wavenumber of the inducing field which is expected to be small for mid-latitude sites. Here, we instead assumed  $Z_u$  to be represented by observations at the island center, which is probably a better approximation because  $Z_i$  tends to vanish in the central region of the island.

The primary approximations implicit in eq. (49) are that,

(1) the electromagnetic response of the ocean is adequately represented by a thin sheet model, and that, (2) the electromagnetic disturbances due to the island are not significantly modified by electromagnetic coupling with the deep conducting regions of the earth. The first condition was discussed in Section 3.3. The essential point is that the electromagnetic continuity conditions must be approximately valid vertically across the ocean. This condition limits the highest frequencies that can be used in the analysis to something like 20 to 50 cpd depending on the deep electrical conductivity conditions (Klein, 1972).

The second condition is associated with the largest uncertainty. Qualitatively, we expect that the disturbed fields will be attenuated vertically ( $z$ ) as  $\exp(-|2\pi z/\lambda|)$ , where  $\lambda$  is a horizontal scale length associated with the disturbed fields, hence with the anomalous bathymetry. This relationship should insure that mutual induction would be small if  $\lambda$  is less than the depth to highly conducting material. Schmucker (1971) demonstrated that this is the case for

a 2-dimensional conductivity inhomogeneity in a thin sheet above a conducting mantle by considering the Fourier transform spectra of the fields. It seems that a similar analysis for a more general thin sheet conductivity distribution should arrive at a similar result.

In the present study a well defined principle axis of induction was found for all near-coastal sites. The principle axis, at all sites was approximately normal to the deep bathymetric contours suggesting that the source of  $Z_i$  is indeed the sea and that  $Z_i$  is not appreciable affected by local conductivity inhomogeneities in the crust or mantle. This conclusion is strengthened in the frequency range lower than 30 cpd by the verification of phase and frequency independent ratios of  $Z_i/H$  between sites. These results imply that  $A$  is constant at a given site and that  $q$  is uniform over the array of stations so that the mantle can be approximated as an isotropic layered medium in this frequency range.

The above results allow us to transfer the data from the various sites to a reference station and thus estimate a single island response spectrum,  $Z_i/H$ . This combination of data strengthens our confidence in the final  $Z_i/H$  estimate and also has the advantage of reducing the unknown quantities to one  $A$  parameter at the reference station and the mantle response spectrum  $q$ .

It is observed that the ratios of  $Z_i/H$  between sites and the axis of principle induction ( $\bar{R}_k$  and  $\bar{\theta}$  in Table 1) can be used to evaluate a numerical model of the island caused field distortions. A theoretical static model of the island distortions was computed

in this study (Appendix I). The theoretical parameters derived are listed in Table 1 with the estimated parameters derived from the data. The discrepancies between the model results and the data are generally larger than the estimated errors in the data. Only sites South and East compare favorably. In the final analysis, the parameter A estimated for the station South was indeed in quite satisfactory agreement with the theoretically predicted value. It is interesting that the data from the sites furthest from the complications of bathymetry of the more western islands of the Hawaiian chain produced estimates of the spatial parameter in closest agreement with the theoretically predicted values. This suggests that the model of the northwestern extension of the Hawaiian Islands may not have been an adequate representation of actual bathymetry (but see Appendix I). These results indicate that theoretical modeling of island magnetic fields must be handled with caution whenever there exists complicated bathymetry on a large scale.

The results of the conductivity modeling show that the present data agree well with Larsen's (1975) model L1 for frequencies up to about 10 cpd. These are the frequencies which overlap between the present data and the Oahu data which Larsen used to interpret model L1. The response function for these low frequencies is influenced primarily by induction in the deep mantle, therefore deep conductivities interpreted with the present data are expected to be similar to those which were interpreted for Oahu. To improve the agreement between the present data and the theoretical response for frequencies higher than 10 cpd, model L1 was modified only in the upper 327 km.

The improved models show that the present data requires a lower conductivity above about 180 km depth than model L1. The maximum conductivity acceptable in this depth range is about .02 mho/m compared to about 0.1 for model L1. A poorly defined additional decrease in conductivity is suggested above about 100 km. The highest conductivity acceptable from about 180 km to 300 km depth is about 0.2 mho/m which is not significantly different from the value of about 0.1 mho/m in model L1.

Although the data put the above mentioned upper bounds on the permissible conductivity structure above 300 km depth, it is found that conductivities are not constrained by a lower bound. This ambiguity with regard to the interpretation of low conductivity is a characteristic of electromagnetic induction studies using noisy and incomplete data. Electromagnetic response functions show increasingly poorer resolution as the structure becomes less conductive, and the problem is worsened when a highly conductive layer (like the ocean) overlies the structure, Schmucker, 1970. Data having greater precision and spanning a larger frequency range is required to alleviate this situation.

Since the required modifications of model L1 primarily affect that part of the response spectrum which has higher frequencies than were used to derive model L1, there is no evidence of a major conductivity inhomogeneity between Oahu and the island of Hawaii.

It should be noted that the present data are insensitive to conductivity inhomogeneities having a scale length less than that of

the island of Hawaii ( $\approx 100$  km). The interpretation of the mantle response depends on the parameter A and the phase dependent relationships of the observed ratio of Z to H, or equivalently, on the relationships between electric currents in the conducting ocean which induce  $Z_1$  and the total H. The oceanic electric currents are expected to be strongly influenced by the resistive island mass, but only weakly distorted by effects of mutual induction with small scale inhomogeneities in mantle conductivity. The conductivity models obtained should therefore be considered as regional averages over a lateral scale of a few hundreds of kilometers. It is therefore not unusual that the present data reflects a conductivity distribution quite similar to that beneath Oahu, Larsen (1975), which is about 300 km northwest. This is true even if one expects smaller scale conductivity anomalies associated with the present volcanism on the island of Hawaii.

The present data in conjunction with experimental data on rock conductivity relationships is able to put rough constraints on the source region for the Hawaiian magma. The spatial distribution of volcanic vents in the Hawaiian Islands suggests a source region of something like 300 km in diameter, Jackson et al. (1972). Jackson et al. (1972) suggest a depth to this source region of about 60 to 100 km. The present data indicate a conductivity at this depth of about .016 mho/m or less. Ignoring pressure effects on conductivity, which seem to be small and using the data on conductivity-temperature relationships for olivine, Duba, Heard, and Shock (1974) this

conductivity implies a maximum temperature of about 1500°C for a crystalline-olivine model. If we assume instead a temperature of about 1200°C, the data implies a maximum melt fraction of about 1%. This is derived from the relationship (Waff, 1974):

$$\phi_m = 150 \sigma / \sigma_m \quad (50)$$

where  $\phi_m$  is the per cent melt having a conductivity  $\sigma_m$  (3.2 mho/m for tholeiitic basalt at 1200°C, Waff, 1974) and  $\sigma$  is the bulk conductivity of the mantle material. These values are to be considered as regional averages over an area having roughly the size of the source region postulated by Jackson et al. (1972).

Thus the present data provides no evidence for a large region ( $\approx 300$  km in diameter) having a significant continuous melt fraction. It may be that zones of concentrated ambient melting or high temperatures are more localized spots in the general source area which are not resolveable using the present data.

The implied melt fraction,  $\approx 1\%$ , seems to be more representative of that suggested for the seismic low velocity zone beneath the lithosphere, Anderson et al. (1972). It is possible that the suggested rise in conductivity at about 100 km correlates with the lower boundary of the lithosphere plate. The resolution of the present data, however, is too poor to conclude anything of certainty about this.

A more definite result of the present study is that the upper 200 km beneath the region of Hawaii Island has a lower mean conductivity than that generally interpreted beneath the oceanic side of continental margins off Peru, California and Japan, Schmucker, 1973. This upper mantle conductivity beneath Hawaii, which seems to be more similar to the normal continental interior regions rather than the tectonically active margins, is indicated both by this study and by Larsen's result (1975). Local perturbations in the upper mantle conductivity structure beneath Hawaii, if present, are more likely to increase the mean conductivity interpretation, rather than decrease it, so the upper 200 km in the mid-oceanic mantle surrounding the Hawaiian volcanic region may be of even lower conductivity than obtained here.

## 7. CONCLUSIONS

A. The differences in the magnetic field variations at various points on the island of Hawaii are attributed to the induction of electric currents in the sea. This is evidenced by the result that the vertical field variations are correlated with horizontal variations on a well defined azimuth that points to the nearest deep ocean. Furthermore, the frequency spectrum of the vertical magnetic variations between sites are related by a real and frequency independent scaling parameter (for frequencies from 2 to 3 cpd).

B. The similarity in the trends of the frequency spectrum of the Z:H response between sites indicates that the main internal part of signal is related to a common deep origin. The fact that those spectrum trends are not strongly dependent on azimuth in the frequency range 2-30 cpd indicates that the mantle can be modeled as an isotropic, laterally uniform conductor to a first approximation.

C. The mantle conductivity found beneath Oahu by Larsen (1975) is consistent with the present data over the lower frequencies in the present data where the two data sets overlap. This is taken to indicate that the deep mantle (300 km and deeper) affects the electromagnetic response similarly on both Oahu Island and the island of Hawaii. In utilizing higher frequencies in the present analysis the model of Larsen (1975) could be refined to show lower conductivities above about 180 km depth. The maximum conductivity to this depth is indicated to be about 0.02 mho/m.

The present data did not constrain the lower bound on electrical conductivity in the upper 180 km of the mantle beneath Hawaii. In this regard it is important that additional electromagnetic studies be attempted in Hawaii and elsewhere in the oceanic areas with emphasis on obtaining a response spectrum over a wider frequency range and with greater precision. Larsen (1975), in analyzing long term data on Oahu, demonstrated that high resolution conductivity interpretations for the deep mantle are possible in the low frequency range ( $< 6$  cpd). Such studies extended to the higher frequencies will help to better resolve the shallower mantle conductivities.

D. Larsen's (1975) analysis, supplemented by the present work, demonstrates that theoretical numerical modeling is not always necessary to account for the electromagnetic field distortions present on oceanic islands. Such modeling helps to understand the nature of the surface induction effects, but it is difficult to predict in this way the correct magnitudes of the parameters of distortion. The analysis of the data as presented here and by Larsen (1975) provides direct estimates of the parameters of the field distortion, and in addition indicates which part of the response spectrum can be considered in the interpretation of deep conductivity by using a layered model of the mantle.

That part of spectrum which we use for interpretation is presently limited to the frequency range where the surface distortions seem essentially static and uncoupled with the deep conductivity. The problem of frequency dependent mutual coupling between the disturbing

fields and the deeper mantle fields remain poorly understood. This is an area where further theoretical investigations will help to clarify the situation. Thin sheet modeling along the lines employed here (Appendix I) but retaining the induction term is one approach. An alternative track is the 2-dimensional Fourier transform method suggested by Schmucker's (1971) work on thin-sheet conductivity anomalies above a conducting substratum.

We note that the method of analysis used here should be applicable to other regions where electromagnetic fields are appreciably influenced by surface conductivity inhomogeneities. It seems, for instance, that magnetotelluric and geomagnetic variation data on continents, Schmucker (1970, 1971, 1973) are often affected by shallow sedimentary structures in a way that could be accounted for by the present analysis rather than by theoretical modeling.

## APPENDIX I

A MODEL OF ELECTRIC CURRENT AND MAGNETIC  
FIELD DISTORTIONS FOR HAWAII ISLAND

## I.1 Theoretical Equations

The basic concepts and assumptions in the thin sheet model of magnetic fluctuations above oceanic island regions are given in Section 3. The starting point here is: (eq. 10, Section 3),

$$\nabla \times \rho \vec{I}_i + i\omega \vec{B}_i = -\nabla \rho \times \vec{I}_u$$

Observe that the fields are partitioned into a uniform part,  $\vec{I}_u$ ,  $\vec{B}_u$ , which are assumed spatially constant, and into an island disturbance part,  $\vec{I}_i$ ,  $\vec{B}_i$  which is assumed to vanish at the outer boundaries of the island region.  $\vec{I}$  is the thin sheet current density,  $\vec{B}$  is the magnetic induction (we designate the vertical component as Z) and  $\rho$  is the inverse of the thin-sheet conductance.

$\vec{I}$  is non-divergent and its vertical component is zero so we can define an electric stream potential  $\phi + \psi$  as,

$$\vec{I} = -\vec{k} \times \nabla(\phi + \psi) \quad (1.1)$$

$\phi$  and  $\psi$  correspond respectively to  $\vec{I}_i$  and  $\vec{I}_u$  with  $\vec{k}$  being the unit vector normal to the thin sheet. If the rectangular coordinates

are oriented so  $\vec{I}_u = I_y \vec{j}$ , the equation (1.1) combines with the first equation above (Price, 1949) to give:

$$\frac{\partial}{\partial x} \left( \rho \frac{\partial \phi}{\partial x} \right) + \frac{\partial}{\partial y} \left( \rho \frac{\partial \phi}{\partial y} \right) - i\omega Z_i = \frac{\partial \rho}{\partial x} \frac{\partial \psi}{\partial x} \quad (1.2)$$

Biot-Savart's law combined with the stream potential of eq. (1.1) (Larsen, 1968), gives for  $Z_i$ ,

$$Z_i(x, y, z) = \frac{\mu}{4\pi} \iint \frac{\nabla \phi(x', y')}{d} \cdot \vec{K} \, dx' dy' \quad (1.3)$$

where,

$$\vec{K} = \int \frac{\vec{F}}{r^3} \, dz'$$

$$\vec{F} = (x-x')\vec{i} + (y-y')\vec{j} + (z-z')\vec{k}$$

$d$  is the mean oceanic depth of the region being modeled. As it stands, eq. (1.3) ignores mantle effects resulting from mutual coupling between the ocean and deep conductivity; however, it is straightforward to generalize this equation to include the effect of a perfectly conducting mantle (Larsen, 1968).

In the present computations the induction term ( $i\omega Z_i$ ) in eq. (1.2) is ignored altogether. This is equivalent to the zeroth order approximation ( $\phi_0, Z_i(\phi_0)$ ) for low frequencies, and

corresponds to the static case. For instance, we can write (Price, 1949),

$$\varphi = \varphi_0 + \alpha \varphi_1 + \alpha^2 \varphi_2 + \dots \quad (1.4)$$

where  $\alpha$  is the coefficient of the integral expression of  $Z_i$  in eq. (1.2). The coefficient  $\alpha$  can be nondimensionalized to the form of

$$\alpha = i\omega\mu\tau_u L \quad (1.5)$$

where  $\tau_u$  is the mean conductance of the deep ocean and  $L$  is a scale length associated with the gradients in  $\rho$ . Equation (1.4) is valid for small  $\alpha$  (Price, 1949) and the zeroth order approximation is expected to be representative of the solution when  $\alpha \ll 1$ . For Hawaii we might typically take  $\tau_u = 15800$  mho and  $L = 100$  km, in which case the zeroth approximation should be adequate for frequencies less than about 8 cpd. Larsen (1975) finds complications in electromagnetic data from Oahu Island for frequencies above about 6 cpd. The present data (Section 5) did not discern problems related to frequency effects below about 30 cpd. Part of the difference may not be real as Larsen worked with remarkably small error tolerances compared to the present data. It can be noted however, that magnetic variations on Oahu exhibit a more complicated behavior than those on Hawaii Island (Klein, 1972).

## I.2 Finite Difference Computations

We desire to satisfy eq. (1.2), without the  $i\omega Z_i$  term, at all points on an  $N \times N$  square net having equidistant grid intervals  $L$ . Figure I-1 shows the grid convention. For notational convenience the nodal locations about  $(j, k)$  are designated as:

$$N = (j - 1, k)$$

$$S = (j + 1, k)$$

$$E = (j, k + 1)$$

$$W = (j, k - 1)$$

$$O = (j, k)$$

Using half-interval central differences based on Taylor series expansions of  $\rho$  and  $\varphi$  about each node "O" we express eq. (1.2) as

$$\begin{aligned} \left(\rho \frac{\partial \varphi}{\partial x}\right)_{N/2} - \left(\rho \frac{\partial \varphi}{\partial x}\right)_{S/2} + \left(\rho \frac{\partial \varphi}{\partial y}\right)_{E/2} - \left(\rho \frac{\partial \varphi}{\partial y}\right)_{W/2} \\ = I_u (\rho_{N/2} - \rho_{S/2}) \end{aligned} \quad (1.6)$$

where  $I_u = \partial \psi / \partial x$  and the quantity  $L^{-1}$  on both sides of the equation is cancelled out. The subscripts refer to the point where a quantity is evaluated, for instance, the subscript "N/2" indicates that the quantity specified is evaluated at the half-interval point between "O" and "N" (see Fig. I-1). By taking the half-interval central differences of the operators on the left-hand side of the

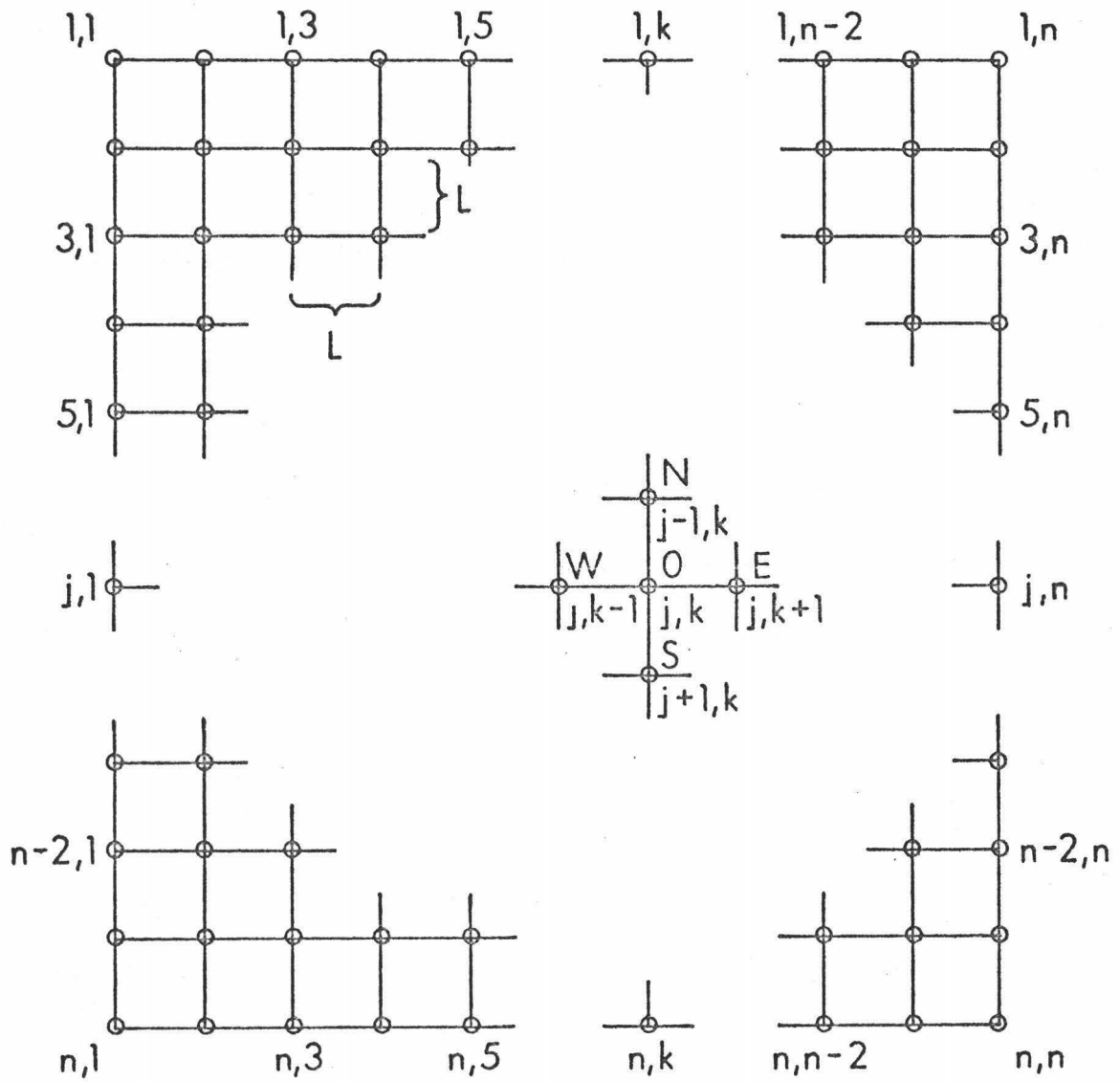


Figure I.1. The grid convention for finite difference calculations.

above equation and approximating the quantities  $\rho_p/\alpha$ ,  
 $p = N, S, E, W$ , by  $(\rho_p + \rho_0)/2$  we find (Sasai, 1968):

$$\begin{aligned} (R_S - R_N) + R_N \phi_N + R_S \phi_S \\ + R_E \phi_E + R_W \phi_W - R \phi_0 = 0 \end{aligned} \quad (1.7)$$

where

$$\begin{aligned} R_p &= \rho_p + \rho_0, \quad p = N, S, E, W \\ R &= \rho_N + \rho_S + \rho_E + \rho_W + 4\rho_0 \end{aligned}$$

and where the intensity of  $I_u$  is defined as  $L^{-1}$  amps. Equation (1.7) is the finite difference approximation to eq. (1.2) that we use to calculate  $\phi$ . We will apply an iterative over-relaxation technique to find  $\phi_{j,k}$  that satisfies eq. (1.7) at all nodes of our grid. The boundary values of  $\phi_{j,k}$  are constant (assumed zero) and the initial internal values of  $\phi_{j,k}$  are arbitrary. Eq. (1.7) at any time in the iterative process, say the  $k$ th iteration, is equal to some residual,  $\epsilon_0^{(k)}$ . The next iteration modifies  $\phi_{j,k}$  to

$$\phi_0^{(k+1)} = \phi_0^{(k)} + W \frac{\epsilon_0^{(k)}}{R} \quad (1.8)$$

where  $W$  is a relaxation parameter,  $1 < W < 2$ , Forsythe and Wasow, 1960, p. 239. The new residual is then

$$\epsilon_0^{(k+1)} = \epsilon_0^{(k)} (1 - W) \quad (1.9)$$

The modification of  $\phi_0$  can be shown to affect the residuals at the adjoining nodes in the following way:

$$\epsilon_p^{(k+1)} = \epsilon_p^{(k)} + W \frac{\epsilon_0^{(k)}}{R}, \quad p = N, S, E, W \quad (1.10)$$

Iterations continue until  $\epsilon_{j,k}$  are sufficiently small. The process is illustrated in the flow chart on Figure II-2. Here  $RES = \epsilon_0$ ,  $ITER = k$ ,  $RO = R$ ,  $PO = W \epsilon_0^{(k)} / R$ . The maximum residual in the net (RMAX) is used to evaluate  $\epsilon_{j,k}$ , SMALL is the preset desired value for RMAX. Iterations are stopped at the iteration ITERMAX if problems in convergence are encountered and RMAX does not go to SMALL.

### I.3 Computation of the Vertical Magnetic Field

Assume that  $\phi_{j,k}$  is known at all nodes of the net described above. The approximation is made that  $\nabla \phi_{j,k}$  is constant within a square of side L centered on each node; then eq. (1.3) can be written as

$$Z_i = \frac{\mu}{4\pi} \sum_p \frac{\nabla \phi_{j,k}}{d} \cdot \vec{G}_p \quad (1.11)$$

where the summation is over all squares, P except the origin where  $Z_i$  is being calculated.  $\vec{G}_p$  is the  $\vec{K}$  term for each node p in eq. (1.3) and is given by:

$$\vec{G}_p = \int_{x'-L/2}^{x'+L/2} \int_{y'-L/2}^{y'+L/2} \frac{\vec{K}}{d} dx' dy' \quad (1.12)$$

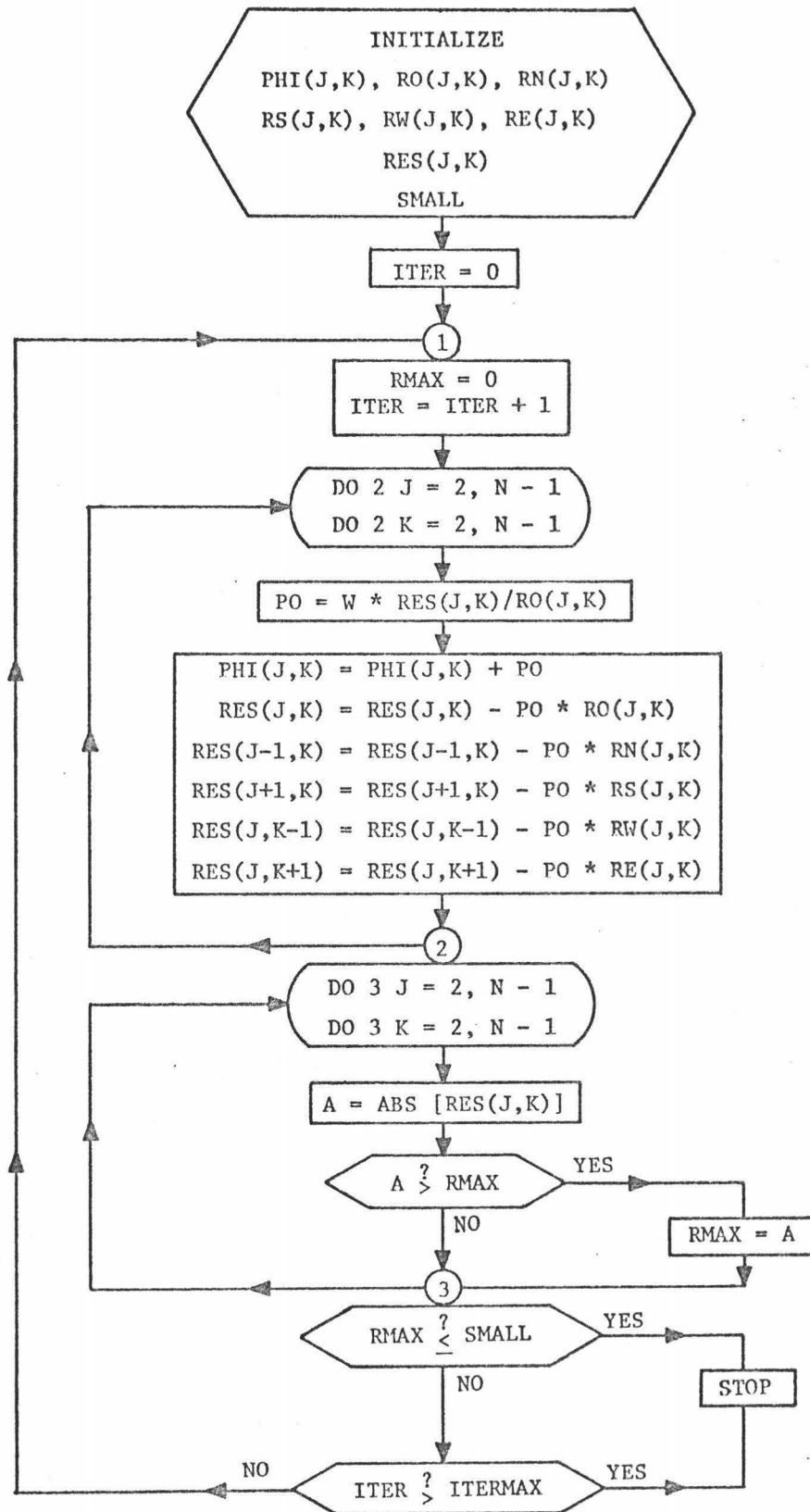


Figure I.2. A flow chart of the finite difference procedure. The variables are defined in the text.

Observe from eq. (1.3) that we need to consider only  $G_x$  and  $G_y$  where for instance (at  $z = 0$  where the limits of integration are deleted)

$G_x$  is given by:

$$G_x = \iint \frac{(x-x')}{R^2(R^2+d^2)^{1/2}} dx' dy' \quad (1.13)$$

where

$$R^2 = (x-x')^2 + (y-y')^2$$

$G_y$  is found by interchanging  $(x - x')$  for  $(y - y')$ . By a change the variables in eq. (1.13) followed by a Taylor series expansion of the integrand, we find approximately,

$$G_x = \int_{u+L/2}^{u-L/2} \int_{v+L/2}^{v-L/2} \left( \frac{u}{(u^2+v^2)^{3/2}} - \frac{ud^2}{2(u^2+v^2)^{5/2}} \right) du dv \quad (1.14)$$

where

$$\begin{aligned} u &= x - x' \\ v &= y - y' \end{aligned}$$

The condition  $d^2/R^2 \ll 1$  is assumed in (1.14). The integrals (1.14) have a closed form, thus  $G_x$  and  $G_y$  can be straightforwardly calculated for each node and inserted into the summation of equation (1.11).

#### I.4 Modeling Results for Hawaii

The numerical model of the static electromagnetic fields about Hawaii was developed in two stages. First, a coarse grid ( $L = 12'$ , approximately 21.5 km) solution was obtained in the region ( $152^{\circ}36'W$ ,  $16^{\circ}N$ ) to ( $161^{\circ}36'W$ ,  $25^{\circ}N$ ). Second, a finer grid solution ( $L = 4'$ , approximately 7.16 km) was found in the region ( $153^{\circ}48'W$ ,  $18^{\circ}N$ ) to ( $156^{\circ}48'W$ ,  $21^{\circ}N$ ). The coarse grid area is roughly centered on the southeastern Hawaiian Islands from the island of Hawaii northwest to the island of Kauai (the most western island in Figure I.3). The fine grid covered the island of Hawaii.

The larger sampling area allowed an approximate solution for the distortions of the electric stream potential caused by the regional features of the Hawaiian Ridge. This regional solution then formed the boundary conditions for the calculation of the fields in the smaller area.

The thin sheet conductance model was based on the ocean depths at the nodes of the grid. These depths were initially digitized directly from a contoured bathymetric chart of the area. In order to obtain a convergent regional solution of the finite difference equations it was necessary to smooth the oceanic depths. Considerable modification of bathymetry was required on the northwestern extension of the Hawaiian Ridge where it intersects the boundary of the model area. The ridge topography was leveled off to the mean ocean depth at the boundary and allowed to slowly reach its true values at about  $160^{\circ}$  west latitude. Similar but less significant modifications were

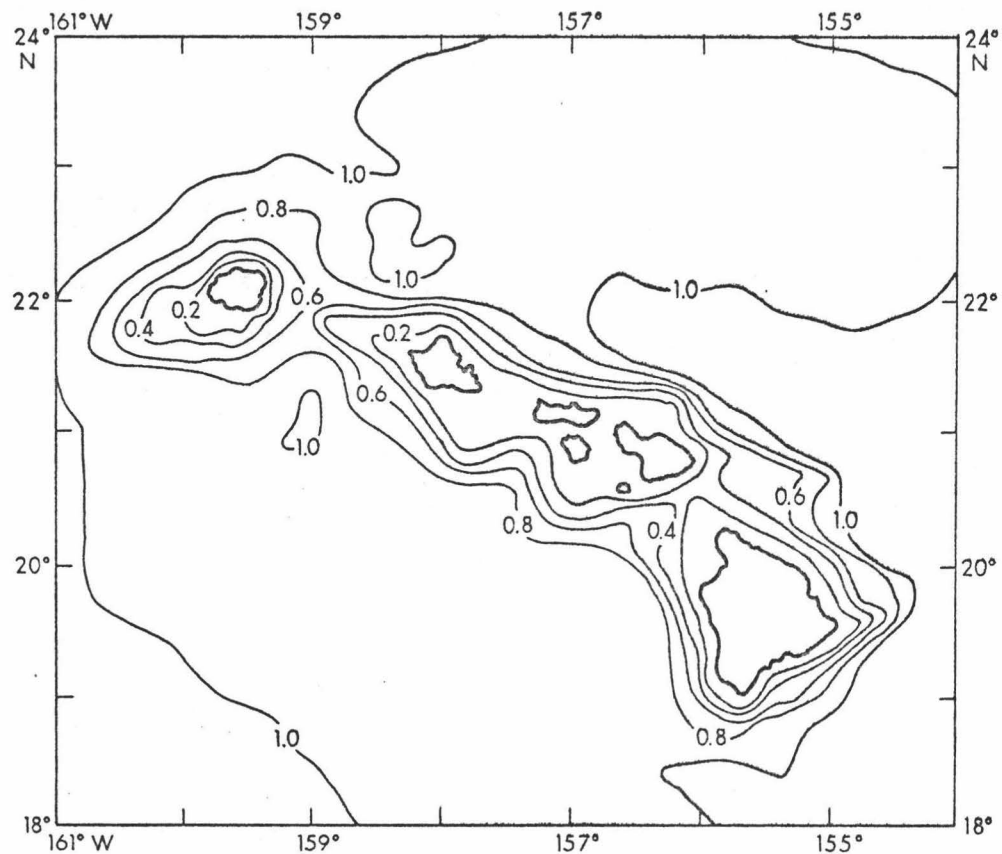


Figure I.3. A generalized conductance map of the Hawaiian Islands. The contours represent the bathymetry normalized to the mean ocean depth on the boundaries, thus they are also roughly equivalent to the normalized vertical conductance of the ocean ( $\text{conductivity} \times \text{depth} \div \text{mean boundary conductance}$ ). The region shown is slightly smaller than the area in which the regional solution of the electric stream function was obtained.

made on the topography for all boundaries. The generalized bathymetric model in the central region of interest is shown in Figure I-3. The depths of this figure are normalized by a mean boundary depth of 4720 m so that this map may be interpreted as a normalized conductance map of the thin sheet model. In the regional calculation the parts of the islands above sea-level were given a normalized conductance of 0.02.

The regional approximation was computed for two orthogonal components of a driving electric current field,  $I_{ux} \vec{i}$  (north-south) and  $I_{uy} \vec{j}$  (east-west). This allows the determination of the distortions relating to any  $\vec{I}_u$  by linearly combining the two computed distortions.

The local distortions, computed on a finer grid and using the regional distortions as boundary conditions, are essentially a refinement of the regional solution. The normalized island conductance in the local computations was set at 0.004.

Figure I-4 shows the final  $(\varphi + \psi)$  on a regional scale for the Hawaii Ridge. Figure I-5 shows the same function in greater detail near Hawaii Island. The electric current flow in these figures parallels the streamlines. The intervals between streamlines represents equal but arbitrary current intensities. The computed vertical magnetic fields are also presented in Figure II-5. The magnitudes of these patterns are normalized to  $\mu_0 I_u$ . These are essentially contour maps of the spatial parameters (a, b) defined

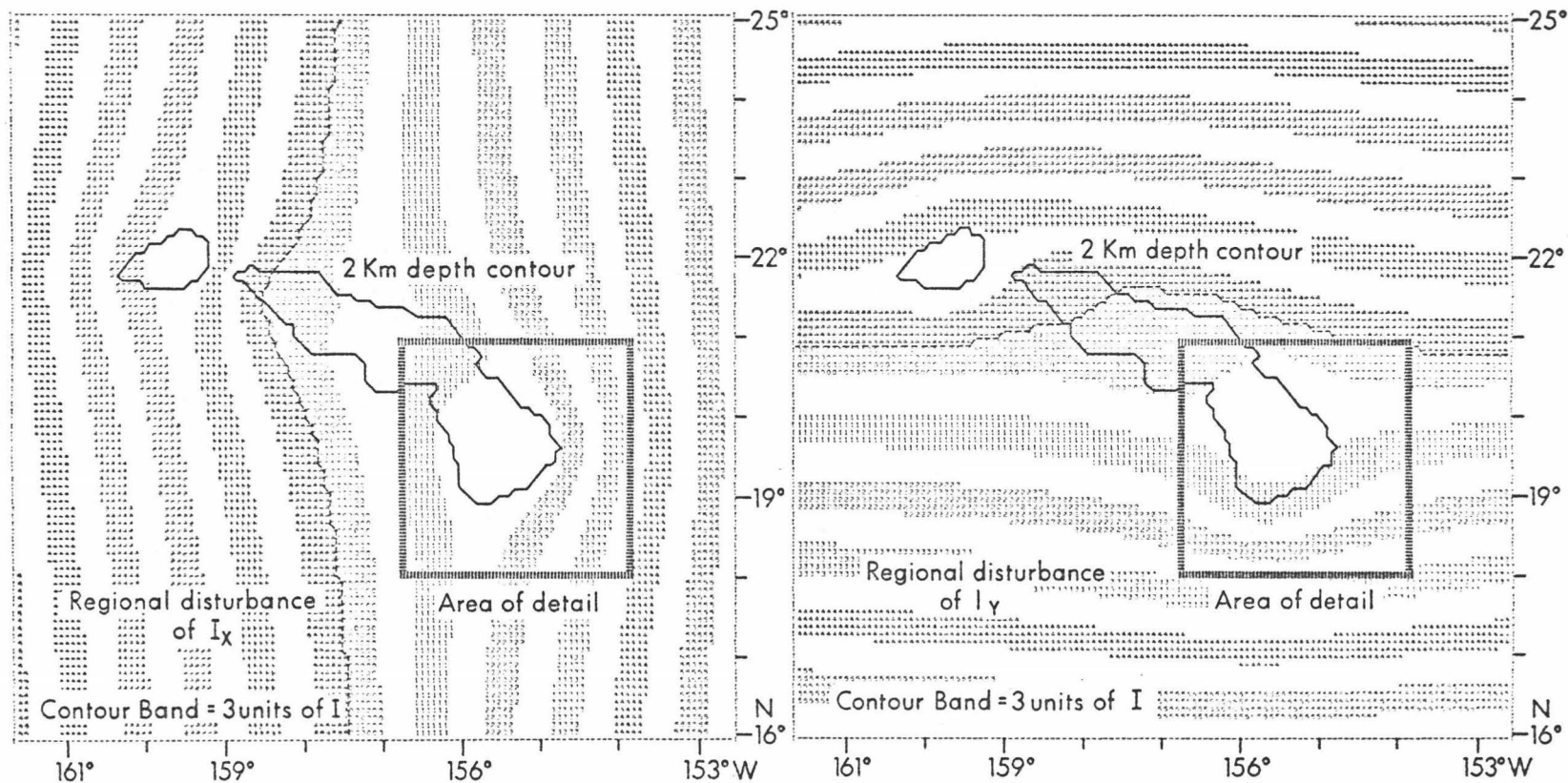


Figure I.4. A model of the regional electric current distortions near Hawaii. This shows the finite-difference solutions of the static uniform current sheet distortions for the cases of north-south directed  $\vec{I}$  ( $I_{ux}$ , left) and east-west directed  $\vec{I}$  ( $I_{uy}$ , right). The area of detail is the region of the finer grid interval solutions shown in Figure I.5 (and Fig. 1, main text).

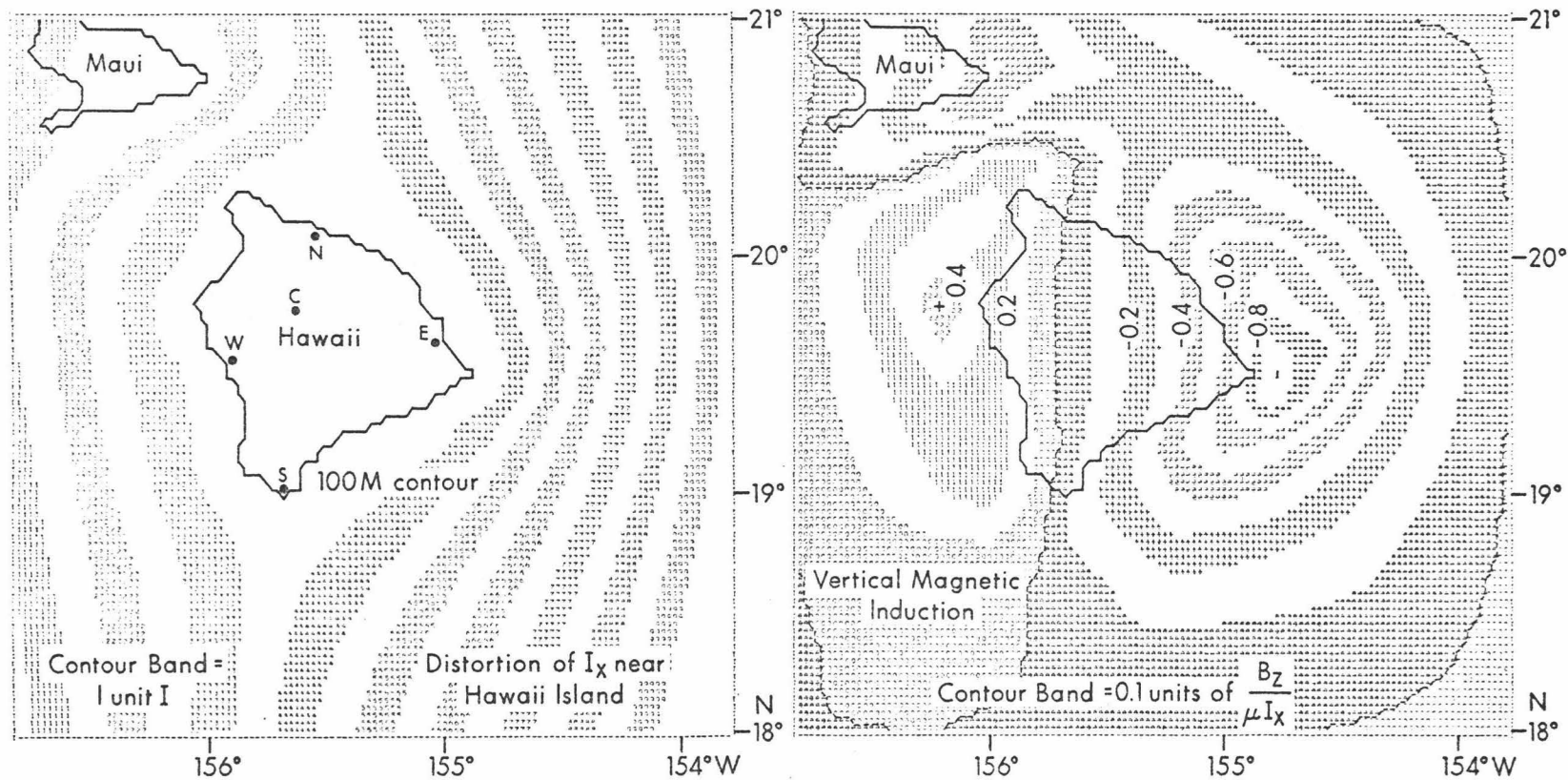


Figure I.5. A model of electric current and magnetic field distortions for Hawaii Island. The units of the electric stream function (left) and the units of the corresponding magnetic field (right) are normalized to the intensity of the uniform current far from the island. The corresponding model for an orthogonally directed driving function is presented in Figure 1 in the main text.

by eq. 11, Section 3:

$$Z_i = \mu (a I_{yu} - b I_{xu})$$

Values for these parameters at the observation sites of this study are listed in Table 1, Section 5.3.

## APPENDIX II

## OBSERVED TIME SERIES AND RESPONSE SPECTRAL ESTIMATES

The basic facts of each of the observation stations are listed in Table II.1. The reduced time-series (Section 5.1) which were analyzed in this report are illustrated in Figures II.1-3. Figure II.4 illustrates the principle axis spectral estimates of the transfer function  $T_{uk}$  and their associated residuals for each site (Section 4.2, especially eq. 30). The subscript "k" indicates the observation site (k = S, N, W, E for sites South, North, West, East respectively). The angle  $\bar{\theta}$  (Section 4.2, eq. 26) is the estimated geographic azimuth of the principle axis of induction for the frequency range below 30 cpd (Table I, Section 5.3). The  $\bar{\theta}$  listed on Figure II.4 are rotated  $180^\circ$  from those in Table I for the purpose of retaining a positive upward axis ( $T_{uk}$ ) in the graphs.

Table II.1. Description of the Geomagnetic Observation Sites

Station, Instrument	Installation Date 1968-1969	Longitude West	Latitude North	Dec.	Elev. (m)	Distance (km)
C-Center (Variograph)	Dec. 5-May 17	155°31.8'	19°45.3'	12°25'	1980	40 - 60
E-East (Fluxgate)	Nov. 1-May 17	155° 4.9'	19°42.2'	10° 6'	43	3
S-South (Fluxgate)	Nov. 5-May 19	155°35.4'	19°38'	11°11'	208	4
W-West (Fluxgate)	Nov. 5-May 18	155°52.9'	19°27.3'	9°34'	372	5
N-North (Fluxgate)	Nov. 2-May 16	155°34.2'	20° 7.2'	13° 7'	232	1

Definition of the parameters:

Dec.: Magnetic declination at each site, East.

Elev.: The elevation from sea level for each site.

Distance: The distance of each site from the coast.

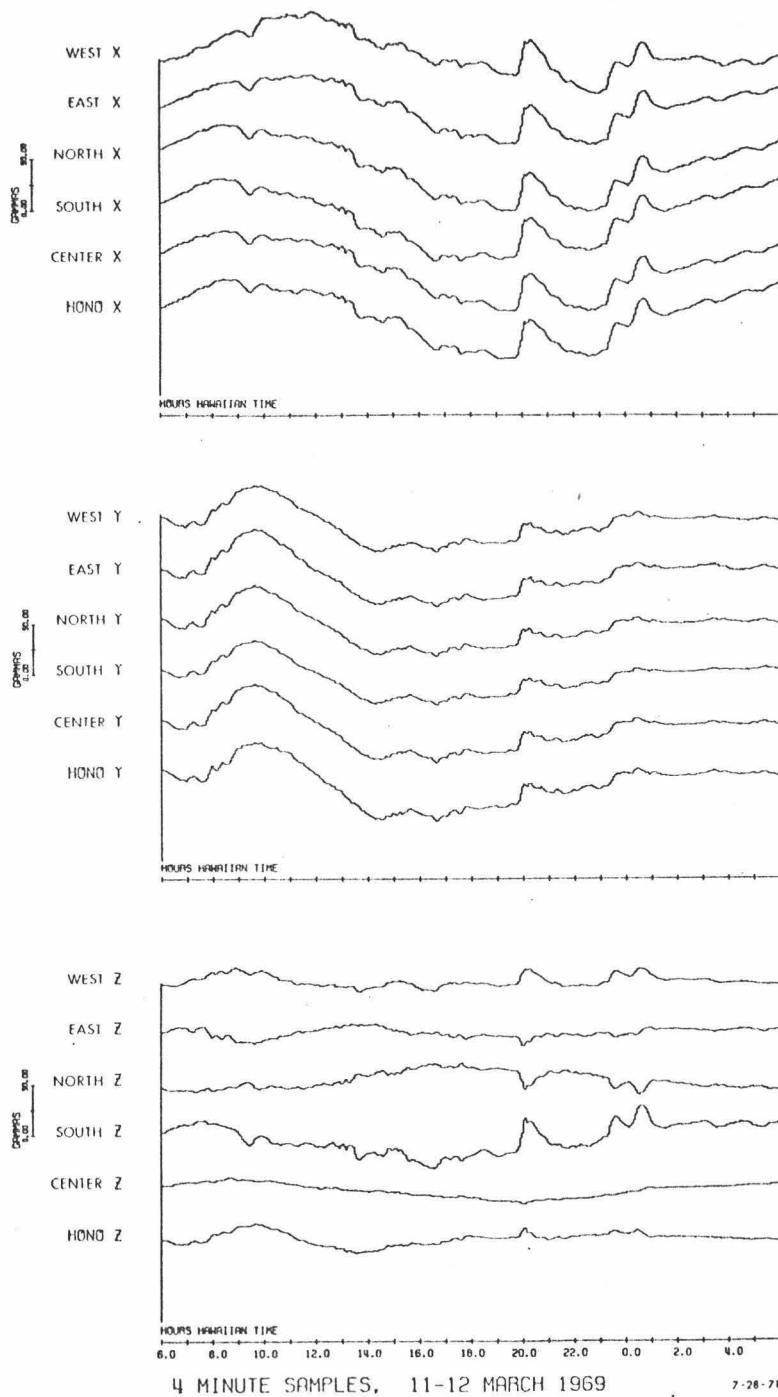


Figure II.1. The 24 hour time-series digitized at 4-minute intervals.

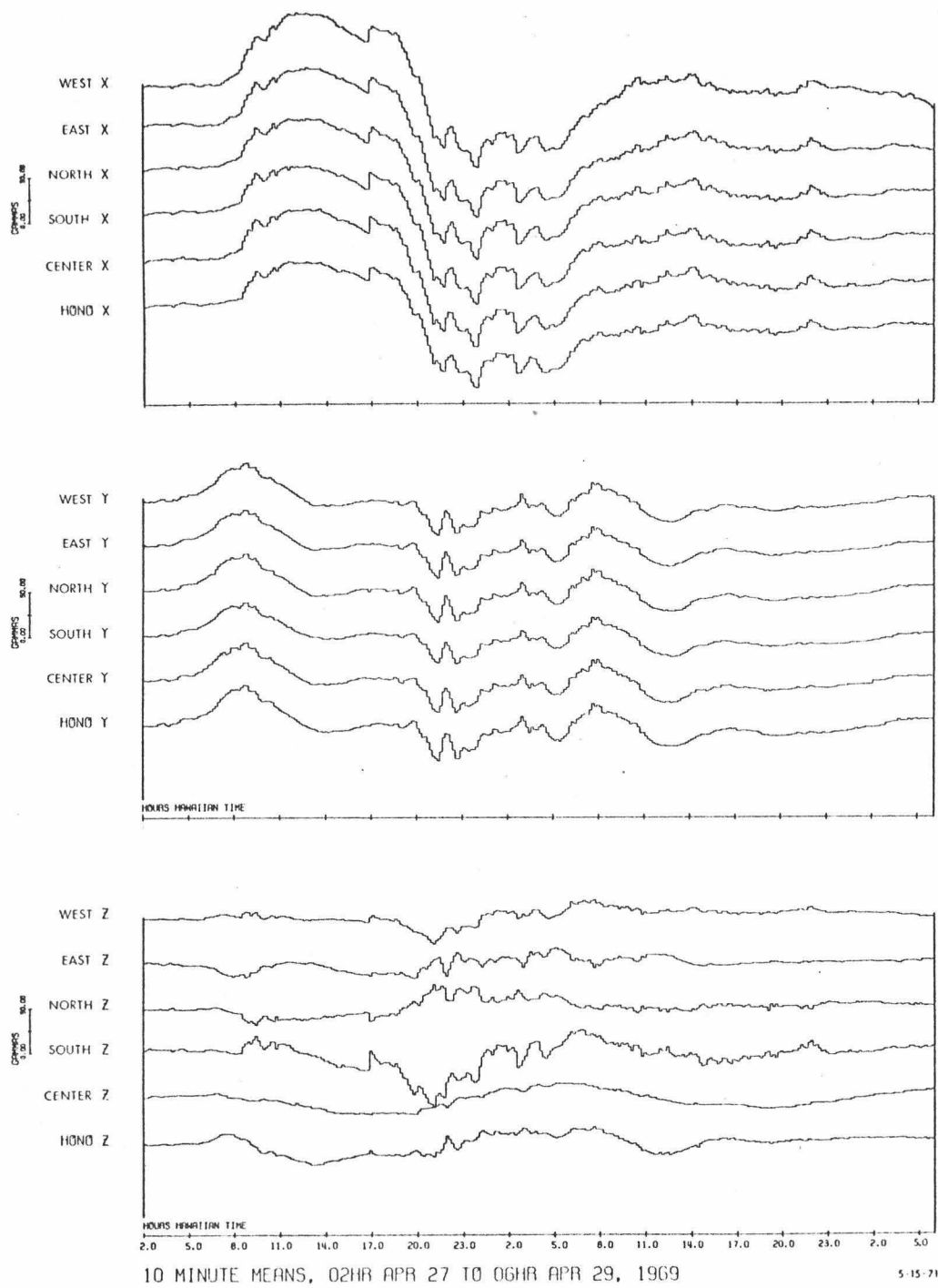
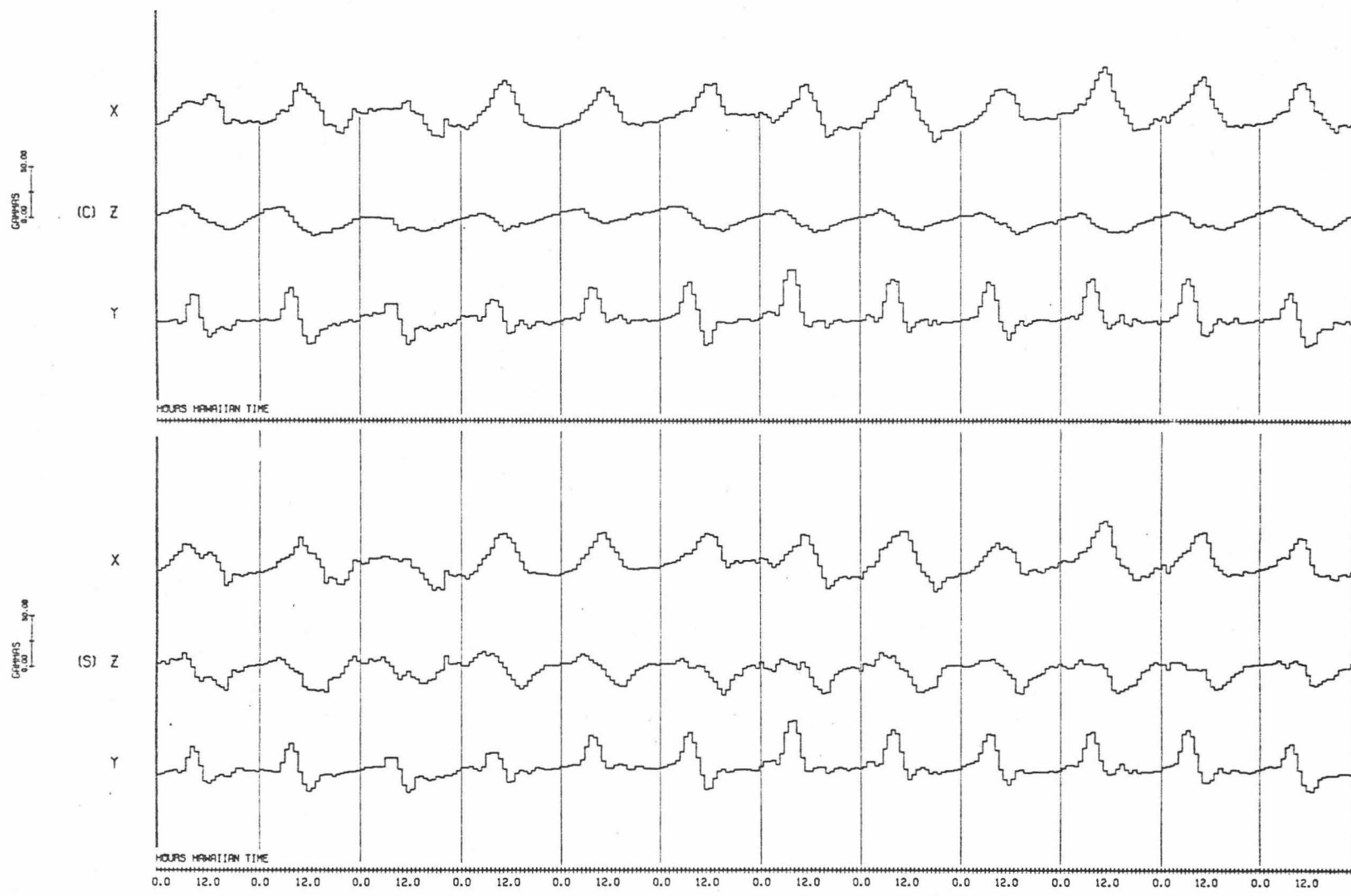
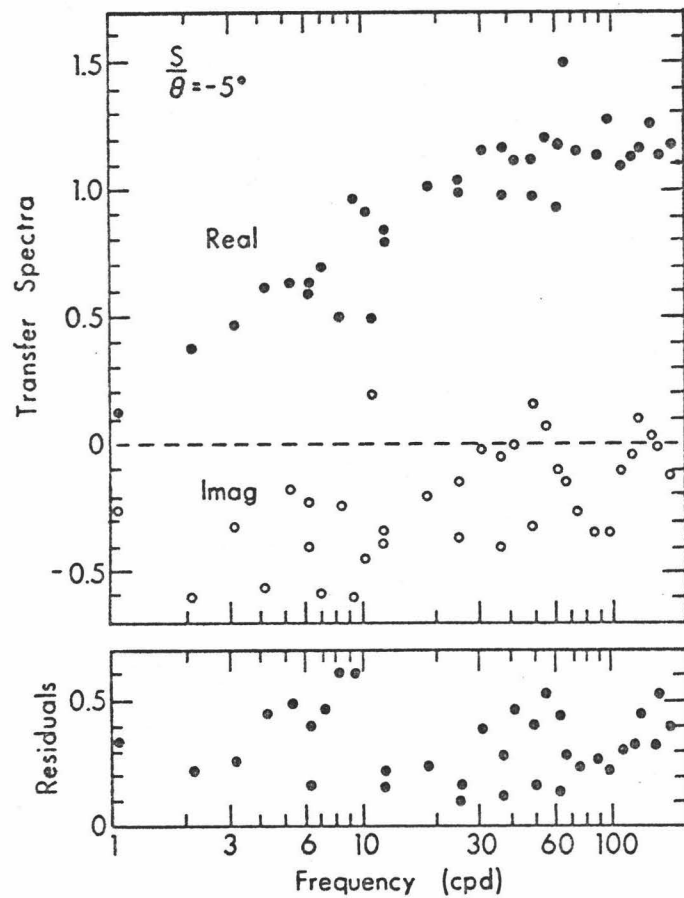


Figure II.2. The 52 hour time-series digitized over 10-minute means.

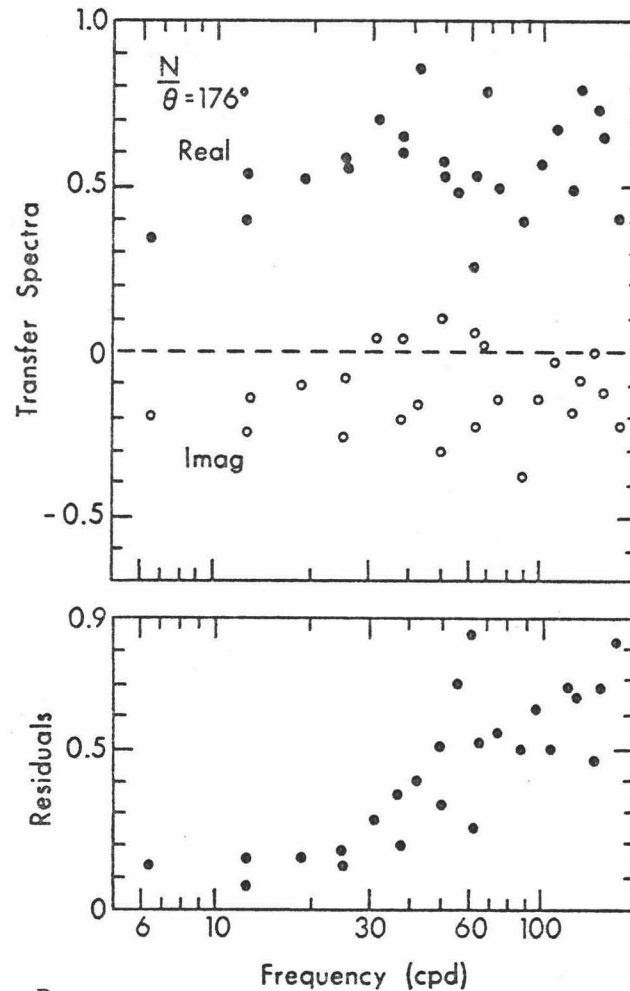


HOURLY MEANS, 00 HR 13 FEB TO 00 HR 25 FEB 1969, HAWAII TIME

Figure II.3. The 12 day time-series digitized over hourly means.

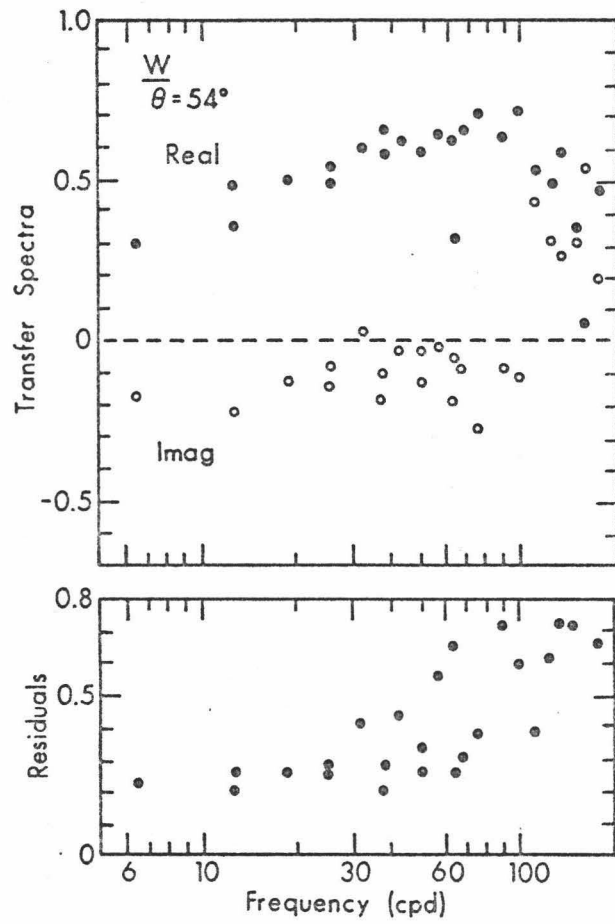


A

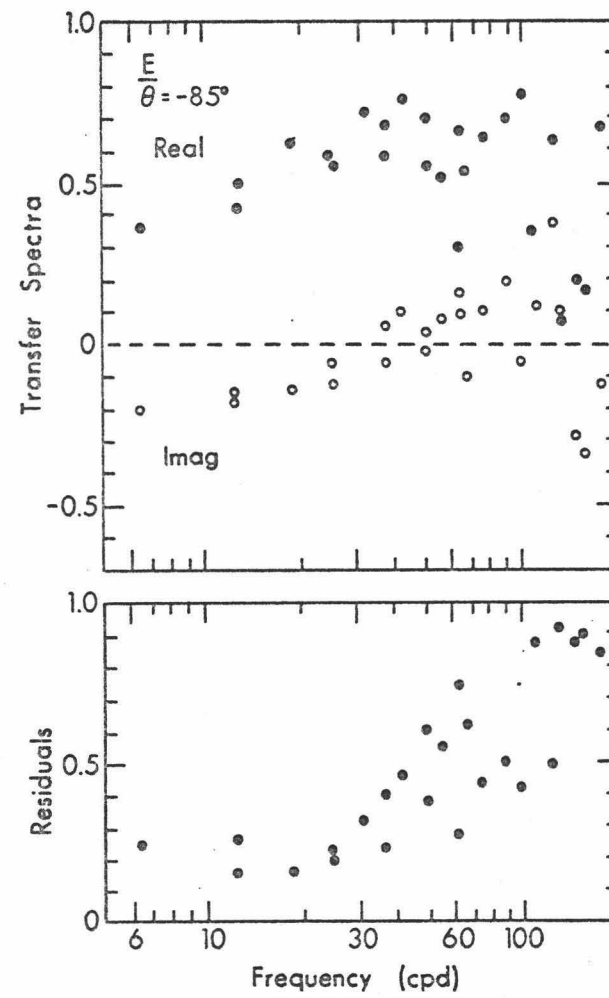


B

Figure II.4. The transfer spectral estimates for each station. The spectra in these figures are rotated to the direction of the estimated azimuth of principle induction ( $\bar{\theta}$ ) for each of the stations S, N, W, E (respectively in Figures II.4a, b, c, d). The spectra and associated residuals for each of the 3 data sets analyzed (Fig. II.1-3) are combined.



C



D

Figure II.4. (continued)

## LITERATURE CITED

- Anderson, D. L., C. Sammis, and T. Jordan, 1972. Composition of the mantle and core, in The Nature of the Solid Earth (Robertson, E. C., ed.), 41-66.
- Bullard, E. C. and R. L. Parker, 1971. Electromagnetic Induction in the Oceans, in The Sea, v. 4, Pt. I (A. E. Maxwell, ed.), Wiley-Interscience, New York, 695-730.
- Duba, A., H. C. Heard, and R. Schock, 1974. Electrical conductivity of olivine at high pressure and under controlled oxygen fugacity, *J. Geophys. Res.* 79, 1667-1673.
- Elvers, D. and D. Perkins, 1964. Geomagnetic research on spatial dependence of time variations across Puerto Rico, (abstr.), *Trans. Amer. Geophys. Un.*, 45, 46.
- Everett, J. E. and R. D. Hyndman, 1967. Geomagnetic variations and electrical conductivity structure in Southwestern Australia, *Phys. Earth Planet. Interiors* 1, 24-34.
- Forsythe, G. E. and W. R. Wasow, 1960. Finite-Difference Methods for Partial Differential Equations, John Wiley, 444 p.
- Honkura, Y., 1971. Geomagnetic variation anomaly on Miyake-Jima Island, *J. Geomag. Geoelect.* 23, 307-333.
- \_\_\_\_\_, 1973 a. Electrical conductivity structure beneath the Islands of Japan as revealed by geomagnetic variation anomalies, D. Sc. Thesis, Univ. of Tokyo.
- \_\_\_\_\_, 1973 b. Island effect and electrical conductivity structure beneath Miyake-Jima Island, *J. Geomag. Geoelect.* 25, 167-179.
- \_\_\_\_\_, S. Oshima, and T. Kondo, 1974. Geomagnetic variation anomaly on Hachijo-jima island, *J. Geomag. Geoelect.* 26, 23-37.
- Jackson, E. D., E. A. Silver, and G. B. Dalrymple, 1972. Hawaiian-Emperor Chain and its relation to Cenozoic circumpacific tectonics, *Geol. Soc. Am. Bull.*, 83, 601-617.
- Klein, D. P., 1971. Geomagnetic time variations on Hawaii Island and mantle electrical conductivity (abstr.), *Trans. Am. Geophys. Un.* 52, 824.

- Klein, D. P., 1972. Geomagnetic time-variations, the island effect, and electromagnetic depth sounding on oceanic islands: results from analysis of data obtained in the frequency range of 0.5 to 10 cycles per hour on Oahu, Hawaii, M.Sc. Thesis, Univ. of Hawaii, Hawaii Inst. of Geophys. Rept. HIG-72-3, 96 p.
- \_\_\_\_\_ and A. Malahoff, 1969. Observations of spatial differences in geomagnetic time-variations on the island of Hawaii (abstr.), Trans. Am. Geophys. Un. 50, 605.
- Larsen, J. C., 1968. Electric and magnetic fields induced by deep sea tides, Geophys. J. 16, 47-70.
- \_\_\_\_\_, 1975. Low frequency (0.1-6.0 cpd) electromagnetic study of deep mantle electrical conductivity beneath the Hawaii Islands, Geophys. J. 43, 17-46.
- Mason, R. G., 1963 a. Spatial dependence of time-variations of the geomagnetic field in the range 24 hours to 3 minutes on Christmas island, unpubl. Rep. 63-3, Geophys. Dept. Imperial College Sci. Technol., London.
- \_\_\_\_\_, 1963 b. Spatial dependence of time-variations of the geomagnetic field on Oahu, Hawaii (abstr.), Trans. Am. Geophys. Un. 44, 40.
- \_\_\_\_\_, 1964. Magnetic effects at Canton island of the 1962 high altitude nuclear tests at Johnston Island, Geophys. Dept. Imperial Coll. Technol., London, Rep. 64-1, 12 p.
- Parkinson, W. D., 1959. Directions of rapid geomagnetic fluctuations. Geophys. J. 2, 1-13.
- Price, A. T., 1949. The induction of electric currents in nonuniform thin sheets and shells, Quart. J. Mech. Appl. Math 2, 283-310.
- \_\_\_\_\_, 1970. The electrical conductivity of the earth. Quart. J. Roy. Astr. Soc. 11, 23-42.
- Rikitake, T., Y. Yukutake, T. Yoshino, Y. Yamazaki, and D. P. Klein, 1969. Observations of geomagnetic variations of short periods on Hawaii Island (in Japanese), Proc. Conductivity Symp. 2, Earthq. Res. Inst., 157-162.
- Rogers, R. A. G., 1966. The effect of islands on electromagnetic induction in the oceans, Ph.D. Thesis, Imperial College, London.

- Sasai, Y., 1968. Spatial dependence of short-period geomagnetic fluctuations on Oshima Island (pt. 2), Bull. Earthq. Res. Inst., Univ. Tokyo 46, 907-926.
- Schumucker, U., 1970. Anomalies of geomagnetic variations in the southwestern United States, Bull. Scripps Inst. Ocean. 13, 165 p.
- \_\_\_\_\_, 1971. Interpretation of induction anomalies above nonuniform surface layers, Geophysics 36, 156-165.
- \_\_\_\_\_, 1973. Regional induction studies: a review of methods and results, Phys. Earth. Planet. Interiors 7, 365-378.
- Schuster, A., 1889. The diurnal variation of terrestrial magnetism, Phil. Trans. R. Soc. London A180, 467-518.
- Tozer, D. C., 1959. The electrical properties of the earth's interior, in Physics and Chemistry of the Earth 3 (L. Ahrens, F. Press, K. Rankama and S. Runcorn, eds.), Pergamon Press, 414-436.
- Waff, H. S., 1974. Theoretical considerations of electrical conductivity in a partially molten mantle and implications for geothermometry, J. Geophys. Res. 79, 4003-4009.
- Wait, J. R., 1970. Electromagnetic waves in stratified media (2nd ed.), MacMillan Co., New York, 372 p.